Dalton Transactions

Accepted Manuscript

ROYAL SOCIETY OF CHEMISTRY

www.rsc.org/dalton

Journal Name

RSCPublishing

ARTICLE

A comparison study of aliphatic and aromatic structure directing agents in influencing the crystal and electronic structures, and property of iodoplumbate hybrids: Water induced structure conversion and visible light photocatalytic property†

Guang-Ning Liu,* Jian-Ru Shi, Xiao-Jiang Han, Xiao Zhang, Ke Li, Jie Li, Tao Zhang, Qi-Sheng Liu, Zhen-Wei Zhang, and Cuncheng Li*

Cite this: DOI: 10.1039/x0xx00000x

Received 00th January 2012,
Accepted 00th January 2012

DOI: 10.1039/x0xx00000x

www.rsc.org/

The invitation of aliphatic amines en (ethylenediamine), aep (N-(2-aminoethyl)piperazine) and tepa (tetraethylenepentamine), and aromatic species 2,2'-bipy (2,2'-bipyridine) and dpe (1,2-di(4-pyridyl)ethylene) as structure directing agents (SDAs) into inorganic iodoplumbates affords six hybrids, namely $[(Hen)_4(H_{2.5}O)_2I](PbI_6)$ (**1**), $Cs_{2n}[Pb_3I_8(en)_2]_n$ (**2**), $(H_3tepa)_n(PbI_5)_n$ (**3**), $(H_2aep)_n(PbI_4)_n$ (**4**), $(Et_2$2,2'-bipy$)_n(Pb_2I_6)_n$ (**5**) and $(Et_2dpe)_n(Pb_2I_6)_n$ (**6**). **1** contains a discrete octahedral $(PbI_6)^{4-}$ anion generated under the direction of a novel co-template $[(Hen)_4(H_{2.5}O)_2I]^{4+}$. **2** contains an inorganic Cs^+ ion and a novel hybrid anionic layer $[Pb_3I_8(en)_2]_n^{2n-}$ that has never been encountered in iodooplumbate hybrids. **3** features a zigzag $(PbI_5)^{3-}$ chain charge compensated by a triprotonated tepa cation. **4** is composed of perovskite sheets of lead(II) octahedra and aep cations that are generated from tepa via an unprecedented in situ ligand reaction. Both **5** and **6** have $(Pb_2I_6)_n^{2n-}$ chains and represent the first example of introducing 2,2'-bipy or dpe derivative cation in iodoplumbate hybrids, respectively. The comparative study reveals that aliphatic amines and aromatic species contribute differently to the crystal and electronic structures, and property of the hybrids. Importantly, **1**–**4** exhibit interesting water induced structure conversions, while **5** and **6** can be used as heterogeneous photocatalysts for dye wastewater treatment under visible irradiation.

1. Introduction

The introduction of organic component into inorganic system to form inorganic-organic hybrid, including hybrid metal halide,[1] chalcogenide,[2] and polyoxometalate[3] has attracted considerable attention due to their abundant crystal and electronic structures, and distinctive properties unavailable in pure inorganic and organic materials. The practical and potential applications in solar cells, chromisms and switchable nonlinear optical (NLO) devices, etc. provide a great motivation for the synthesis and property study of metal halide based hybrids.[1,4,5,6] In hybrid materials, the organic moieties not only as charge compensation agents balance the negative charge on the inorganic moieties, but also as structure directing agents (SDAs) influence the structures of the inorganic framework. Although it has been demonstrated that the organic moieties with different size, charge, shape, as well as hydrogen bond sites heavily influence the crystal and electronic structures, and physical properties of hybrid materials, a clear relationship between them still not observed, and hence a sustained effort on the synthesis and property study of hybrid materials is necessary.

Aliphatic amines and aromatic organic species are two types of mainly used SDAs, which exhibit different structural and physical features from each other. The former are typically flexibility, linear and easily soluble in water, while the latter are generally rigid, flat, and photo/electrochemical active. These obvious differences engender aliphatic amines and aromatic organic species having different contributions to the structure and property of metal halide based hybrids. For example, aliphatic amines could direct the formation of metal halide based hybrids with perovskite type structures that have application in photovoltaic cells with power conversion efficiency now exceeds 18%.[4] Also, the flexibility of the aliphatic amines may cause structural or conformational changes when temperature changes, which could lead to reversible phase transitions and potential applications in dielectric and NLO switch of metal halide based hybrids.[5] For aromatic SDAs, besides the unusual contributions to the crystal and electronic structures of metal halide hybrids, they can also produce additional or improved physical properties to the hybrids. It has been reported that the utilization of functional aromatic species as SDAs can bring in optical properties such as photochromism or thermochromism behaviors that are novel

in metal halide based hybrids.[1c,6] However, it should be noted that although lots of work have systematically studied aliphatic or aromatic SDAs with different substituents in influencing the structures and properties of metal halide based hybrids,[5c,7] their work were usually performed on either aliphatic or aromatic SDAs. A comparison study of aliphatic and aromatic SDAs in influencing the structure and property of metal halide based hybrids is rarely reported.[8]

Aliphatic chelating polyamines such as en (ethylenediamine), dien (diethylenetriamine), tren (triethylenetetramine), tepa (tetraethylenepentamine) and 1,2-dac (1,2-hexamethylene diamine) have been widely used in the syntheses of hybrid chalcogenides and polyoxometalates.[9] Although related work has also performed in metal halide based hybrids, additional transition metal (TM) ions were usually added in the reaction systems, where chelating polyamines typically coordinate to the TM ions to generate metal complex cations as SDAs.[10] We have been interested in the comparison study of aliphatic amines and aromatic species as SDAs in influencing the structure and property of metal halide hybrids.[8] In hybrid haloargentates, we demonstrated that aromatic SDA, $(H_2dpe)^{2+}$ (dpe = 1,2-di(4-pyridyl)ethylene), could direct the formation of a novel β-type $(AgI_2)^-$ anionic chain and adjust the band gap in a way different from aliphatic amines.[8] In this work, with the aim to compare the different contributions of aliphatic amines (no TM ions added in the reaction systems) and aromatic species to the structure and property of iodoplumbate hybrids, we select aliphatic chelating polyamines en, dien, tren, tepa and 1,2-dac, and aromatic pyridine-based species 2,2'-bipy (2,2'-bipyridine) and dpe as SDAs to synthesize iodoplumbate hybrids. Six hybrid compounds were successfully isolated,[11] namely $[(Hen)_4(H_{2.5}O)_2I](PbI_6)$ (**1**), $Cs_{2n}[Pb_3I_8(en)_2]_n$ (**2**), $(H_3tepa)_n(PbI_5)_n$ (**3**), $(H_2aep)_n(PbI_4)_n$ (**4**), $(Et_2$2,2'-bipy$)_n(Pb_2I_6)_n$ (**5**), and $(Et_2dpe)_n(Pb_2I_6)_n$ (**6**), which show diverse structures with different dimensionalities: 0-D (zero-dimensional) for **1**, 1-D for **3** and **5**–**6**, and 2-D for **2** and **4**. Compound **1** features a novel co-template $[(Hen)_4(H_{2.5}O)_2I]^{4+}$ directing the formation of a discrete octahedral $(PbI_6)^{4-}$ anion. Compound **2** contains inorganic Cs^+ ions and a novel hybrid anionic layer $[Pb_3I_8(en)_2]_n^{2n-}$ that has never been encountered in iodoplumbate hybrids. Compound **3** contains a zigzag $(PbI_5)^{3-}$ chain charge compensated by a letter "C"-like triprotonated tepa cation. Compound **4** is composed of perovskite sheets of lead(II) octahedra, and aep cations that are generated from tepa molecules via an unprecedented in situ ligand reaction. Compounds **5** and **6** contain the same inorganic $(Pb_2I_6)_n^{2n-}$ anionic chain and represent the first example of introducing 2,2'-bipy and dpe derivative cation in iodoplumbate systems, respectively. The comparative study reveals that aliphatic amines and aromatic species contribute differently to the crystal and electronic structures, and properties of the iodoplumbate hybrids. Importantly, compounds **1**–**4** exhibit interesting water induced structure conversions, while **5** and **6** are stable in water and can be used as heterogeneous photocatalysts for dye wastewater treatment under visible irradiation. Herein, we report the detailed syntheses, crystal and electronic structures, water induced structure conversions (for **1**–**4**) and visible light photocatalytic degradations of organic dye (for **5**–**6**).

2. Experimental section

2.1 Materials and physical measurements

All reagents were purchased commercially and used without further purification. Elemental analyses of C, H, and N were performed on an Elementar Vario EL III microanalyzer. Powder X-ray diffraction (PXRD) patterns were recorded on Bruker D8 Focus diffractometer using Cu $K\alpha$ radiation. A Perkin-Elmer Diamond thermogravimetric analyzer was used to obtain thermogravimetric analyses (TGA) curves in N_2 with a flow rate of 20 mL/min and a ramp rate of 10 °C·min^{-1} in the temperature range 30–1000 °C. An empty Al_2O_3 crucible was used as the reference. The FT-IR spectra were obtained on a Perkin-Elmer spectrophotometer using KBr disk in the range 4000–400 cm^{-1}.

2.2 Photocatalytic experiments

The evaluation of photocatalytic activities of compounds **5** and **6** for the photocatalytic decolorization of organic dye was performed at ambient temperature. The procedure was as follows: 0.020 g of powder sample was dispersed into 40 mL of methyl orange (MO, 14.2 mg L^{-1}) aqueous solution for 30 min in the absence of light to attain adsorption-desorption equilibrium, followed by the addition of one drop of hydrogen peroxide solution (H_2O_2, 30%). A 300 W xenon arc lamp was used as a light source. An optical filter in the equipment of xenon arc lamp was used to filtering out the UV emission below 400 nm. Visible light then irradiated the above solutions. During the degradation, the mixture was stirred continuously by means of a magnetic stirrer. The samples were withdrawn regularly from the reactor, and dispersed powders were removed by centrifugation. At different time intervals, analytical samples were withdrawn and analyzed by UV/Vis spectroscopy.

2.3 Computational details

The X-ray crystallographic data of **2**–**6** was used to calculate its electronic structure. The calculations of density of states (DOS) were carried out using density functional theory (DFT) with one of the three nonlocal gradient-corrected exchange-correlation functionals (GGA-PBE) and performed with the CASTEP code,[12] which uses a plane wave basis set for the valence electrons and norm-conserving pseudopotential for the core electrons.[13] The number of plane waves included in the basis was determined by a cutoff energy, E_c, of 280 eV for **2**–**6**. Pseudo-atomic calculations were performed for Pb $5d^{10}6s^26p^2$, I $5s^25p^5$, Cs $5s^25p^66s^1$, C, $2s^22p^2$, N $2s^22p^3$ and H $1s^1$. The parameters used in the calculations and convergence criteria were set by the default values of the CASTEP code.[12]

2.4 Preparations for 1–6

Preparation for 1. A mixture of PbI_2 (0.231 g, 0.50 mmol), ethanediamine (1.0 mL), ethanol (2.0 mL) and concentrated HI (45%, 3.0 mL) was heated at 180 °C for four days in a sealed 25-mL Teflon-lined stainless steel vessel. Upon cooling to room temperature, colorless chip crystals of **1** were obtained in 70% yield (based on PbI_2). Elemental analysis calcd. (%) for $C_8H_{41}I_7N_8O_2Pb$: C 6.98, H 3.00, N 8.14; found: C 7.29, H 2.97, N 7.96. IR (KBr pellet, cm^{-1}) 3447(m), 3321(w), 3077(vs), 3011(vs), 2481(vw), 2344(vw), 1949(vw), 1580(s), 1472(s), 1311(w), 1013(s), 966(m), 948(m), 804(m), 769(m), 673(vw), 572(w), 471(w).

Preparation for 2. A mixture of PbI_2 (0.231 g, 0.50 mmol), CsCl (85 mg, 0.48 mmol), ethanediamine (1.0 mL), ethanol (2.0 mL) and concentrated HI (45%, 3.0 mL) was heated at 160 °C for four days in a sealed 25-mL Teflon-lined stainless steel vessel. Upon cooling to

room temperature, colorless block crystals of **2** were obtained in 91% yield (based on PbI_2). Elemental analysis calcd. (%) for $C_4H_{16}Cs_2I_8N_4Pb_3$: C 2.38, H 0.80, N 2.77; found: C 2.77, H 0.95, N 3.24. IR (KBr pellet, cm^{-1}) 3830(w), 3471(m), 3262(m), 3202(s), 3112(m), 2595(w), 2918(s), 2865(w), 2342(vw), 2140(vw), 2035(vw), 1557(vs), 1437(m), 1310(m), 1123(s), 1018(vs), 966(s), 861(m), 622(m), 615(w), 488(s).

Preparation for 3. A mixture of PbI_2 (0.231 g, 0.50 mmol), tetraethylenepentamine (1.0 mL), ethanol (2.0 mL) and concentrated HI (45%, 3.0 mL) was heated at 150 °C for four days in a sealed 25-mL Teflon-lined stainless steel vessel. Upon cooling to room temperature, colorless prismatic crystals of **3** were obtained in 87% yield (based on PbI_2). Elemental analysis calcd. (%) for $C_8H_{26}I_5N_5Pb$: C 9.29, H 2.53, N 6.77; found: C 9.72, H 2.17, N 6.62. IR (KBr pellet, cm^{-1}) 3436(m), 3293(m), 3239(m), 3060(vs), 2893(vw), 2833(w), 1563(s), 1455(vs), 1389(w), 1312(m), 1229(m), 1127(m), 1044(w), 996(s), 852(w), 811(m), 752(s), 483(m).

Preparation for 4. A mixture of PbI_2 (0.231 g, 0.50 mmol), tetraethylenepentamine (1.0 mL), ethanol or H_2O (2.0 mL) and concentrated HI (45%, 3.0 mL) was heated at 180 °C for seven days in a sealed 25-mL Teflon-lined stainless steel vessel. Upon cooling to room temperature, orange block crystals of **4** were obtained in 83% yield (based on PbI_2). Elemental analysis calcd. (%) for $C_6H_{17}I_4N_3Pb$: C 8.52, H 2.03, N 4.97; found: C 8.75, H 2.07, N 4.87. IR (KBr pellet, cm^{-1}) 3452(m), 3059(vs), 2825(w), 2414(w), 2341(vw), 1640(vw), 1550(s), 1454(vs), 1411(w), 1387(s), 1308(m), 1178(s), 1133(m), 1072(m), 1090(s), 1066(m), 1042(m), 988(s), 874(s), 824(m), 752(m), 572(w), 517(vw).

Preparation for 5. A mixture of PbI_2 (0.231 g, 0.50 mmol), 2,2'-bipy (0.156 g, 1.00 mmol), ethanol (2.0 mL) and concentrated HI (45%, 2.0 mL) was heated at 190 °C for six days in a sealed 25-mL Teflon-lined stainless steel vessel. Upon cooling to room temperature, yellow block crystals of **5** were obtained in 90% yield (based on PbI_2). Elemental analysis calcd. (%) for $C_{14}H_{18}I_6N_2Pb_2$: C 12.10, H 1.31, N 2.02; found: C 12.19, H 1.37, N 2.21. IR (KBr pellet, cm^{-1}) 3441(s), 3036(s), 2977(w), 2929(w), 2344(vw), 1867(vw), 1610(vs), 1581(s), 1485(vs), 1461(vs), 1384(w), 1294(w), 1157(s), 1068(m), 1090(s), 1031(vw), 966(vw), 900(vw), 644(vw), 549(vw), 465(vw).

Preparation for 6. A mixture of PbI_2 (0.231 g, 0.50 mmol), dpe (0.090 g, 0.50 mmol), ethanol (8.0 mL) and concentrated HI (45%, 1.0 mL) was heated at 160 °C for seven days in a sealed 25-mL Teflon-lined stainless steel vessel. Upon cooling to room temperature, red prismatic crystals of **6** were obtained in 93% yield (based on PbI_2). Elemental analysis calcd. (%) for $C_{16}H_{20}I_6N_2Pb_2$: C 13.57, H 1.42, N 1.98; found: C 13.42, H 1.47, N 1.86. IR (KBr pellet, cm^{-1}) 3434(m), 3043(w), 2932(w), 1629(vs), 1518(m), 1455(s), 1337(w), 1201(m), 1169(s), 1071(vw), 964(m), 839(s), 556(m).

Compounds **1**–**6** are stable in dry air and insoluble in common organic solvents. The phase purities of bulk crystals of **1**–**6** for physical property measurements were confirmed by PXRD studies (Fig. S1). The experimental PXRD patterns are in good agreement with the simulated patterns from the single-crystal structures, which reveals the phase purity of the bulk crystalline materials.

2.5 Single-crystal structure determination

The intensity data sets of **1**–**6** were collected on a Agilent Xcalibur, Eos, Gemini CCD diffractometer equipped with a graphite-monochromated Mo $K\alpha$ radiation (λ = 0.71073 Å) at 293 K. The data sets were reduced by the CrysAlisPro[14] program. An empirical absorption correction using spherical harmonics was implemented in SCALE3 ABSPACK scaling algorithm. The structures were solved by direct methods using the Siemens SHELXL package of crystallographic software.[15] The difference Fourier maps created on the basis of these atomic positions to yield the other non-hydrogen atoms. The structures were refined using a full-matrix least-squares refinement on F^2. All non-hydrogen atoms were refined anisotropically. The Hydrogen atoms were located at geometrically calculated positions and refined as riding on their parent atoms. All the protons were located from a different Fourier synthesis. For the monoprotonated en molecule ($N2H_2$-$C2H_2$-$C3H_2$-$N3H_2$) in **1**, the H^+ was assigned to one terminal -NH_2 group. For the other two monoprotonated en molecules, the H^+ was assigned to both terminal -NH_2 groups with an occupancy of 50%. Crystallographic data and structural refinements for **1**–**6** are summarized in Table 1. Important bond lengths and angles are listed in Table S1.

Table 1. Crystal and Structure Refinement Data for **1**–**6**.

	1	**2**	**3**
Formula	$C_8H_{41}I_7N_8O_2Pb$	$C_4H_{16}Cs_2I_8N_4Pb_3$	$C_8H_{26}I_5N_5Pb$
M_r (g mol^{-1})	1376.98	2022.80	1034.03
Crystal system	Monoclinic	Orthorhombic	Monoclinic
Space group	*C*2/c	*C*mca	$P2_1$/n
ρ_{calcd} [g cm^{-3}]	2.763	4.420	3.007
a [Å]	15.3294(3)	19.6228(13)	15.4571(5)
b [Å]	9.4774(2)	14.0896(8)	8.8221(4)
c [Å]	23.2087(6)	10.9953(5)	16.7663(9)
α [°]	90	90	90
β [°]	101.006(2)	90	92.382(4)
γ [°]	90	90	90
V [$Å^3$]	3309.81(13)	3040.0(3)	2284.35(18)
Z	4	4	4
T [K]	293(2)	293(2)	293(2)
F(000)	2456	3392	1824
θ range [°]	2.61–26.73	2.57–25.50	3.35–25.50
Measured reflections	8930	5343	11239
Independent reflections (R_{int})	3488 (0.0286)	1458 (0.1010)	4232 (0.0291)
Data/params/restraints	3022/132/9	1047/55/0	3656/172/0
R_1[a], wR_2[b] [$I>2\sigma(I)$]	0.0488, 0.1490	0.0674, 0.1649	0.0241, 0.0472
Goodness of fit	0.993	0.996	1.020
$\Delta\rho_{max}$ and $\Delta\rho_{min}$ [e $Å^{-3}$]	1.363, –1.398	4.784, –3.230	0.930, –0.880

	4	5	6
Formula	$C_6H_{17}I_4N_3Pb$	$C_{14}H_{18}I_6N_2Pb_2$	$C_{16}H_{20}I_6N_2Pb_2$
M_r (g mol^{-1})	846.02	1390.08	1416.12
Crystal system	Orthorhombic	Orthorhombic	Monoclinic
Space group	*P*bca	*P*bca	$P2_1/c$
ρ_{calcd} [g cm^{-3}]	3.314	3.345	3.093
a [Å]	18.2273(7)	18.1430(6)	10.8414(4)
b [Å]	8.9569(4)	15.7880(5)	18.2977(6)
c [Å]	20.7698(8)	19.2737(8)	7.9777(2)
α [°]	90	90	90
β [°]	90	90	106.088(4)
γ [°]	90	90	90
V [Å^3]	3390.9(2)	5520.8(3)	1520.58(8)
Z	8	8	2
T [K]	293(2)	293(2)	293(2)
F(000)	2944	4784	1224
θ range [°]	2.72–25.49	2.72–25.50	3.04–25.50
Measured reflections	9947	17407	8816
Independent reflections (R_{int})	3145 (0.0761)	5112 (0.0405)	2825 (0.0293)
Data/params/restraints	2517/127/0	3700/217/0	2347/118/0
R_1[a], wR_2[b] [$I>2\sigma(I)$]	0.0529, 0.1346	0.0389, 0.0773	0.0310, 0.0678
Goodness of fit	1.003	0.992	1.003
$\Delta\rho_{max}$ and $\Delta\rho_{min}$ [e Å^{-3}]	3.452, –2.427	1.236, –1.802	0.850, –0.981

[a] $R_1 = \sum||F_o|-|F_c||/\sum|F_o|$, [b] $wR_2 = \{\sum w[(F_o)^2-(F_c)^2]^2/\sum w[(F_o)^2]^2\}^{1/2}$

3. Results and discussion

3.1 Synthetic considerations

Aliphatic chelating polyamines including bidentate en and 1,2-dac, tridentate dien, tetradentate tren and pentadentate tepa, and aromatic pyridine-based species 2,2'-bipy and dpe were selected to synthesize iodoplumbate hybrids under solvothermal conditions. Although we have tried our best to vary the reaction conditions, not all the aliphatic chelating polyamines were successfully incorporated into inorganic iodoplumbates (scheme 1). Compounds **1**, **3**, and **4** with protonated en, tepa and aep (formed via an in situ ligand reaction) cations were obtained. The addition of Cs^+ ion in the reaction system of **1** affords compound **2**, which features an inorganic Cs^+ ion charge compensating an unprecedented hybrid anionic layer $[Pb_3I_8(en)_2]_n^{2n-}$. Obviously, the introduction of Cs^+ cation makes en molecule free from acting as a charge compensating agent, but act as a neutral chelating ligand to Pb atom in the hybrid anionic layer. Similar efforts by adding additional Cs^+ ion in the reaction systems of **3**–**6** are unable to obtain new phases. Moreover, the attempts of replacing Cs^+ with other cations with smaller or larger radius e.g., K^+, Rb^+ or $(CH_3)_4N^+$ cation to get new phases in the synthesis of **2** were unsuccessful. All these suggest that only the Cs^+ ion with proper radius could collaborate with en molecule to co-direct the formation of iodoplumbate hybrid.

In situ ligand reaction under solvo(hydro)thermal conditions has provoked significant interest for discovering new organic reactions and making novel compounds.[16] Of particular interest, an unprecedented in situ ligand reaction has been observed in this work. The reaction condition of **4** has resulted in the in situ cyclization of tepa molecule to aep molecule presumably due to an intramolecular cyclization reaction (Scheme 2). The syntheses of **3** and **4** with the same starting materials but under different reaction temperatures (150 °C for **3** and 180 °C for **4**) strongly suggests that temperature greatly influence the in situ cyclization reaction. Further, an extension of the reaction time to seven days is needed for the synthesis of **4**, because it can significantly increase the yield. Similar cyclization reactions of aliphatic chelating polyamines can be observed elsewhere.[17] In case of tepa, the cyclization reactions to generate 4-(2-aminoethyl)-triethylenetetramine and N-(2-aminoethyl)piperazine-1,4-diethylamine have been reported recently,[17h] however the intramolecular cyclization to generate N-(2-aminoethyl)piperazine like that in **4** has never been observed.

<Please insert scheme 1 here>

Scheme 1. The synthetic route of **1–6**.

<Please insert scheme 2 here>

Scheme 2. Possible cyclization reaction mechanism of a tepa molecule.

3.2 Crystal structures

Compounds **1**–**6** feature 0-D (for **1**), 1-D (for **3**, **5** and **6**) or 2-D (for **2** and **4**) structures containing isolated or polymerized (PbI_6) octahedra. The Pb-I bond lengths varying in normal ranges 3.1965(3)–3.2906(3) Å for **1**, 3.1711(4)–3.2202(3) Å for **2**, 3.0896(3)–3.3180(2) Å for **3**, 3.1397(3)–3.2831(3) Å for **4**, 3.1197(4)–3.4005(4) Å for **5** and 3.2118(3)–3.2670(3) Å for **6**, and the I-Pb-I bond angles (adjacent iodides) deviating from the ideal value of 90° (Table S1) indicate the distortions of the (PbI_6) octahedra, which suggests the $6s^2$ electronic lone pairs on Pb(II) ions in **1**–**6** are more or less stereochemically active.[1b,18]

Crystal structure of 1. Single-crystal X-ray diffraction analysis reveals that compound **1** crystallizes in the monoclinic space group *C*2/c and is composed of isolated octahedral $(PbI_6)^{4-}$ anion, protonated en and water cations, and I^- anion (Fig. 1). The protonated en, water cations together with iodine anion as a whole direct the assembly of inorganic iodoplumbates anion, revealing obvious cooperative directing effects. In other words, compound **1** can be considered to be formed under direction of the co-template of organic cation (protonated en), inorganic cation (protonated water), and inorganic anion (I^-). There is only one crystallographically independent Pb atom, which is coordinated by six I atoms, in a slightly distorted octahedral coordination environment. The Pb–I bond distances (3.1965(3)–3.2906(3) Å) are comparable with those found in other iodoplumbate hybrids containing discrete $(PbI_6)^{4-}$ anion.[19] The I1, I1A, I3 and I3A (A: (1-x, y, 3/2-z)) reside in the equatorial positions, and the apical positions are occupied by the I2 and I2A atoms with the axial angle of I2–Pb1–I2A of 177.80(1)°, as opposed to the ideal angle of 180°. The en and H_2O molecules were assigned protonated to compensate the negative charges of the $(PbI_6)^{4-}$ and I^- anions. Interestingly, the protonated en molecules in **1** adopt two different configurations with the C–C and C–N bond distances in their normal ranges (Fig. S2).[20] Supramolecular assembly through the hydrogen bond is an efficient route to create materials with designed structures and properties. In **1**, the co-template contains fo+ur

protonated en molecules, two protonated water molecules and one I^- anion, wherein each I^- anion interacts with two protonated en via N–H···I hydrogen bonds, and each protonated water molecule connects with three protonated en cations via O–H···I hydrogen bonds, and connects with one neighboring protonated water via O–H···O hydrogen bond to form a 2-D supramolecular layer parallel to the *ab* plane (Fig. S3a, Table S2). Each octahedral $(PbI_6)^{4-}$ anion using its four equatorial I atoms connects with six $(Hen)^+$ cations of the co-template through N–H···O hydrogen bonds to form a 3-D supramolecular framework (Figs. S3b and S3c).

An important structural feature of **1** is the existence of a novel co-template formed by organic cations $(Hen)^+$, inorganic cations $(H_{2.5}O)^{0.5+}$, and inorganic anions I^- through supramolecular interactions. Hybrid halometallates synthesized by employing co-templates of solvent molecule + organic cation,[21] organic anion + organic cation,[20a] and inorganic anion + organic cation have been reported,[22] however the co-template like that in **1** has never been reported up to now.

<Please insert Fig. 1 here>

Fig. 1 The crystal structure of **1**. Hydrogen atoms are omitted for clarity. Symmetry codes: A (1-x, y, 3/2-z); B (-x, 1-y, 1-z); C(1-x, 1-y, 1-z).

Crystal structure of 2. Compound **2** crystallizes in the orthorhombic space group *C*mca and contains isolated Cs^+ ions, and 2-D hybrid anionic structures formed by Pb^{2+} cations, I^- anions and en molecules (Fig. 2). There are three quarters of Pb atom (one forth of Pb1 and one half of Pb2), one half Cs^+ ion, two I^- anions, and one half en molecule in the asymmetric unit of **2**. Pb1 and Pb2, Cs1, I2, and I3 atoms are all in special positions. Both Pb1 and Pb2 atoms are six-coordinated, but in different coordination geometries. The Pb1 atom is coordinated by four μ_2-I and two I_t atoms (I_t = terminal I) to form a slightly distorted ($Pb1I_6$) octahedron. The Pb2 atom is six-coordinated by two N atoms from one chelating en ligand, and four μ_2-I atoms to form a ($Pb2I_4en$) unit. The Pb–μ_2-I bond distances in the range of 3.2079(2)–3.2202(3) Å are noticeable longer than the Pb–I_t bond distance of 3.1711(4) Å. The ($Pb2I_4en$) units corner-share with each other via two μ_2-I atoms to form novel hybrid chains $(PbI_4en)_n$ extending along the *c* direction. The octahedral ($Pb1I_6$) anion as an inorganic linker shares four μ_2-I atoms with two adjacent hybrid chains and connects the chains into hybrid 2-D anionic layers $[Pb_3I_8(en)_2]_n^{2n-}$ parallel to the *ac* plane (Fig. S4a). The isolated Cs^+ ions reside between the anionic layers charge-compensating the negative charges of the anionic layers (Fig. S4b). Careful inspection of the crystal structure indicates that there are electrostatic forces rather than hydrogen bonds between the anionic layers. Instead, N-H···I hydrogen bonds are observed within the 2-D hybrid layer (Figs. S4b and S5, Table S3).

The most remarkable structural feature of **2** is the existence of a novel hybrid 2-D anionic layer formed by inorganic (PbI_6) linkers connecting hybrid $(PbI_4en)_n$ chains. As is well-known, inorganic 2-D iodoplumbate anionic layers e.g., $(PbI_4)^{2-}$,[7b,23] $(Pb_3I_{10})^{4-}$,[24] and $(Pb_4I_{18})^{10-}$[20a] are very common in iodoplumbate hybrids. Contrastively, 2-D iodoplumbate anions with covalent bonded organic species showing a hybrid characteristic are rarely reported, and so far can only be observed in six compounds,[25] however where the hybrid layers are all formed by organic ligands or metal organic complex cations as linkers connecting inorganic $(Pb_xI_y)^{(y-2x)-}$ chains, showing a different hybrid feature from that in **2**.

<Please insert Fig. 2 here>

Fig. 2 The crystal structure of **2**. Hydrogen atoms are omitted for clarity. Symmetry codes: A (1-x, y, z); B (x, 1-y, 2-z); C (1-x, 1-y, 2-z); D (1/2-x, 1-y, 1/2+z); E (1/2-x, y, 3/2-z); F (x, 1-y, 1-z); G (1/2-x, 1-y, -1/2+z); H (1/2-x, y, 1/2-z).

Crystal structure of 3. Compound **3** crystallizes in the monoclinic space group $P2_1/n$ and contains a 1-D zigzag $(PbI_5)^{3-}$ chain and a triprotonated tepa cation. The asymmetric unit of **3** is composed of one $(PbI_5)^{3-}$ unit (part of a zigzag chain of corner-sharing octahedra), and one triprotonated tepa cation (Fig. 3). The Pb1 atom is in a typical octahedral coordination environment, formed by two μ_2-I atoms (I1, I1A) and four terminal I atoms (I2, I3, I4 and I5). The octahedron shares two adjacent corners to form an infinite zigzag single chain extending along the *b* direction with the Pb1–μ_2-I–Pb1B bond angle of 165.93(1)° and the μ_2-I1–Pb1–μ_2-I1A bond angle of 84.68(1)°. The Pb–μ_2-I bond distances varying from 3.2904(3)–3.3180(2) Å and the Pb–I_t bond distances in the range 3.0896(3)–3.2537(3) Å are in their normal ranges. The tepa molecules curve with the shape similar to the letter "C", and are triprotonated to reach charge neutralization of the structure of **3**. The "C"-like tepa molecules clamp both sides of the $(PbI_5)^{3-}$ chain, and interact with the inorganic chain via N–H···I and C–H···I hydrogen bonds to form a 1-D neutral hybrid supramolecular chain (Fig. S6a, Table S4). Such hybrid chains are stacked and form C–H···I hydrogen bonds with neighboring ones to form 2-D supramolecular layers parallel to the (101) plane (Fig. S6b), which are further stacked each other along the [101] direction through the electrostatic forces to form a 3-D supramolecular framework (Fig. S6c).

The 1-D $(PbI_5)^{3-}$ single chain is not unusual in iodoplumbate hybrids,[5a,7a,7d,18,26] where two isomers of $(PbI_5)^{3-}$ can be observed. One is the linear type formed by each (PbI_6) octahedron shares opposite corners;[5a,18,26a] the other is the zigzag type formed by (PbI_6) octahedra alternatively share opposite corners and adjacent corners.[7a,7d,26b,26c] In **3**, the $(PbI_5)^{3-}$ single chain adopts the zigzag type. Additionally, it should be noted that compound **3** represents the first example of introducing tepa derivative cation in iodoplumbate hybrid.

<Please insert Fig. 3 here>

Fig. 3 The crystal structure of **3**. Hydrogen atoms are omitted for clarity. Symmetry codes: A (1/2-x, -1/2+y, 3/2-z); B (1/2-x, 1/2+y, 3/2-z).

Crystal structure of 4. Compound **4** crystallizes in the orthorhombic space group *P*bca and features N-(2-aminoethyl)piperazine cationic single layers separated by single-layer-thick perovskite sheets of lead(II) octahedra. Four unique iodine atoms surround the lead atom in the asymmetric unit with the Pb–I bond distances in their normal ranges (Fig. 4). I1 and I3 are in axial positions; I2 and I4 and their symmetry equivalent I2A (1/2-x, -1/2+y, z) and I4B (-x, 1/2+y, 1/2-z) lie in the equatorial plane and are shared between the octahedra. The Pb–I bond distances to the axial halides with the average value of 3.1686(3) Å is about 0.0887 Å shorter than the average value of the bridging Pb–I bond of 3.2573(3) Å. The two unique bridging I atoms, I2 and I4, introduce two bridging angles Pb1–μ_2-I2–Pb1 of 153.87(1)°, and Pb1–μ_2-I4–Pb1 of 163.26(1)°. The former angle is noticeable more acute than the latter one, and both are more acute compared to the similar angle Pb1–μ_2-I–Pb1 of 165.93(1)° in **3**. In corner-sharing (PbI_6) octahedra of **4**, the trans angle formed by two axial I atoms is 175.49(1)°, and those formed between four bridging halides are 170.592(8)° and 175.609(8)°, which are all deviating from the ideal case of 180°. In the crystal structure of **4**, each gap made by four corner-sharing (PbI_6) octahedra is occupied above and below by two $(H_2aep)^{2+}$ cations that are arranged in a head-tail mode of the piperazine head and ethylamine tail. The halogen ions in the axial positions together with one of the bridging iodides connects with the $(H_2aep)^{2+}$ cations via N–H···I and C–H···I hydrogen bonds (Fig. S7a, Table S5), which form the inorganic layers sandwiching the organic cationic layers (Fig. S7b).

Although tepa molecules were used as SDAs in the reaction of **4**, structural analysis identifies the presence of biprotonated aep cations in the product, which suggests that the reaction condition has resulted in the cyclization of tepa molecules leading to in situ formation of aep. Such in situ intramolecular cyclization of tepa to generate aep has never been reported before.

<Please insert Fig. 4 here>

Fig. 4 The crystal structure of **4**. Hydrogen atoms are omitted for clarity. Symmetry codes: A (1/2-x, 1/2+y, z); B (1/2-x, -1/2+y, z); C (-x, -1/2+y, 1/2-z); D (-x, 1/2+y, 1/2-z).

Crystal structure of 5. Compound **5** crystallizes in the orthorhombic space group *P*bca and is composed of $(Et_2$2,2'-bipy$)^{2+}$ cation and 1-D infinite $(Pb_2I_6)_n^{2n-}$ anionic chain (Fig. 5). The infinite $(Pb_2I_6)_n^{2n-}$ chain extends along the *b* direction and consists of trans face-sharing (PbI_6) octahedra, which have two crystallographic independent Pb atoms and six I atoms. The Pb–I bond distances range from 3.1197(4) to 3.4005(4) Å, and the I–Pb–I bond angles fall in the range of 167.509(9)–177.649(9)° for trans type and 83.565(8)–104.341(9)° for cis type, which are consistent with those found in other $(Pb_2I_6)_n^{2n-}$ chains.[20b,27] The crystal packing of **5** clearly displays each 1-D iodoplumbate chain is encapsulated in each trapezoid channel formed by $(Et_2$2,2'-bipy$)^{2+}$ cations extending along the *b* direction (Fig. S8). Unlike the flexible aliphatic amines in **1**–**4**, which form plenty of hydrogen bonds with inorganic iodoplumbates. Structural analysis indicates that the shortest C···I distance of 3.724(4) Å and N···I distance of 3.797(3) Å both are longer than the sum of their van der Waals radii, indicating that there are electrostatic forces instead of hydrogen bonds between $(Et_2$2,2'-bipy$)^{2+}$ cations and $(Pb_2I_6)_n^{2n-}$ anionic chains. The 2,2'-bipy species in **5** has two nearly perpendicular pyridyl rings with the dihedral angle of 81.033(115)°, and are bi-ethylated generating $(Et_2$2,2'-bipy$)^{2+}$ cation to counter the negative charges on the $(Pb_2I_6)^{2-}$ anionic chain. Further, the nearest centroid to centroid distance between the pyridyl rings of two neighbouring $(Et_2$2,2'-bipy$)^{2+}$ cations is 5.441(1) Å indicating that there is no significant π···π stacking interaction.

Aromatic 2,2'-bipy has been used to synthesize iodoplumbate hybrids by others, however it usually forms TM complex cations as SDAs[27d,28] or as a chelating ligand chelates to the inorganic iodoplumbate skeleton[29] in reported compounds. Compound **5** represents a rare example of discrete 2,2'-bipy derivative cation as SDA in a iodoplumbate hybrid.

<Please insert Fig. 5 here>

Fig. 5 The crystal structure of **5**. Hydrogen atoms are omitted for clarity. Symmetry codes: A (1/2-x, -1/2+y, z).

Crystal structure of 6. Compound **6** crystallizes in the monoclinic space group $P2_1/c$ and contains inorganic infinite $(Pb_2I_6)_n^{2n-}$ chains and bi-ethylated dpe cations $(Et_2dpe)^{2+}$ (Fig. 6). The asymmetric unit has one Pb atom, three I atoms, and one half $(Et_2dpe)^{2+}$ cation. The Pb and I atoms form inorganic $(Pb_2I_6)_n^{2n-}$ anionic chain similar to that in **5**. However, the invitation of bigger aromatic bi-ethylated dpe cations in **6** leads to a decrease in crystallographic symmetry (No. 61 for **5** and No. 14 for **6**) and different orientations of the inorganic iodoplumbate anionic chains: along the *b* axis in **5** and *c* axis in **6**. Besides, the Pb–I bond distances (3.2118(3) to 3.2670(3) Å), and the I–Pb–I bond angles (169.738(8)–174.383(11)° for trans type and 84.248(8)–100.529(10)° for cis type) in **6** all show a narrower range compared with those in **5**, which implies that the $(Pb_2I_6)_n^{2n-}$ anionic chain in **6** is less distorted than that in **5**. The crystal packing diagram of **6** can be described as each $(Pb_2I_6)_n^{2n-}$ anionic chain encapsulated in each channel formed by $(Et_2dpe)^{2+}$ cations extending along the *c* direction (Fig. S9). Similar to **5**, there are electrostatic forces instead of hydrogen bonds between aromatic organic cations and inorgnaic anionic chains. Notably, the organic components interact with the inorganic components via electrostatic forces both in **5** and **6**, which is different from the hydrogen bond interactions in **1**–**4**. This may ascribe to the more flexible skeleton and more hydrogen bond sites of aliphatic amines in **1**–**4** than pyridine-based organic species in **5** and **6**. Because linked by a ethenyl, the two pyridine rings in the dpe molecule are nearly coplanar with dihedral angle of 0.0(1)°. The centroid to centroid distance

between the pyridyl rings of two neighboring $(Et_2dpe)^{2+}$ cations is too long (minimum value of 5.404 Å) to generate significant π···π stacking interaction.

Although aromatic dpe derivative cations have been observed in other metal halide based hybrids e.g., hybrid iodoargentates[8,30] and hybrid iodocuprates,[31] to our knowledge, dpe derivative cation directing the formation of hybrid iodoplumbate has never been reported before.

<Please insert Fig. 6 here>

Fig. 6 The crystal structure of **6**. Hydrogen atoms are omitted for clarity. Symmetry codes: A (x, 1/2-y, 1/2+z); B (x, 1/2-y, -1/2+z); C (1-x, 1-y, -z).

The different influences of aliphatic amines and aromatic species to the crystal structures of iodoplumbate hybrids. Aliphatic amines with flexible skeleton and more than one $-NH_2$ or >NH groups (which can form abundant hydrogen bonds with solvent molecule to form co-templates or with the inorganic iodoplumbate anions) are likely to occur unpredictable behaviors during the solvothermal syntheses of metal halide hybrids, as exemplified by the syntheses of **1**–**4** where unpredictable behaviors include aliphatic amines hydrogen bonding with solvent or inorganic ions to form a novel co-template in **1**, acting as a neutral organic ligand chelating to the inorganic iodoplumbate skeleton in **2**, been tri-protonated to form a charge compensation agent with a charge of +3 in **3** (mono- or bi-protonated with positive charge of +1 or +2 are common for aliphatic amines), and undergoing in situ ligand reaction in **4**. Unpredictable behaviors of aliphatic amines may enable them to direct the formation of more abundant inorganic iodoplumbate anions. In this work, aliphatic amines direct the formation of hybrid iodoplumbates with anionic structures varing from 0-D $(PbI_6)^{4-}$ octahedral anion, 1-D $(PbI_5)_n^{3n-}$ anionic chain to 2-D $[Pb_3I_8(en)_2]_n^{2n-}$ hybrid layer or $(PbI_4)_n^{2n-}$ inorganic layer. Contrastively, the aromatic pyridine-based organic cations direct the formation of **5** and **6** in this work with iodoplumbate anion only including $(Pb_2I_6)_n^{2n-}$ anionic chains. From the analysis above, it seems that employing aliphatic amines as SDAs are more likely to generate metal halide hybrids with unpredictable crystal structures. However, it should be noted that besides SDAs, other important factors including the temperature, solvent, pH value of the solution, and the molar ratio of the reactant can also greatly influence the crystal structures of the hybrids.

3.3 Optical spectroscopy

In the IR spectra of **1**–**6** (Fig. S10), the IR bands at 3340–3280 cm^{-1} and 2540–2315 cm^{-1} for **1** are attributed to the $N–H^+$ deformation and stretching vibrations of the protonated en molecules. For **3** and **4**, the IR bands at 2870–2810 cm^{-1} and 2550–2320 cm^{-1} are attributed to the $N–H^+$ stretching vibrations of the triprotonated tepa and biprotonated aep molecules. For **5**–**6**, the strong bands in the region of 3010–3070 cm^{-1} correspond to the C–H vibrations of the aromatic ring hydrogen atoms, ν(=C–H). The bands of ring vibrations of the aromatic N-heterocyclic species (ν(C=C) and ν(C=N)) are observed at 1455–1630 cm^{-1}. The broad bands in the range of 3525–3435 cm^{-1} for **1**–**6** are assigned to the stretching of trace water since the measurements were conducted in air.

Solid state UV-vis absorption spectra of **1**–**6** and inorganic bulk PbI_2 calculated from the diffuse reflectance data by using the Kubelka-Mulk function are plotted in Fig. 7. It can be seen that the band gaps of **1**–**6** can be divided into two groups compared with the measured value of 2.30 eV for bulk PbI_2. Compounds **1**–**3** and **5** have bigger band gaps of 2.87 eV for **1**, 3.05 eV for **2**, 2.85 eV for **3**, and 2.64 eV for **5** exhibiting an observed blue shift compared with the band gap of bulk PbI_2. While, compounds **4** and **6** have smaller band gaps of 2.20 eV for **4** and 2.16 eV for **6**, thereby showing an observed red shift compared with that of bulk PbI_2. Our previous comparison study in iodoargentate hybrids reveals that aliphatic amine-containing hybrids generally have bigger band gaps than those of aromatic species-containing hybrids.[8] In this work, the band gaps of **1**–**3** follow the rule having bigger band gaps than **5** and **6**. However, compound **4** does not follow the rule and has a smaller band gap. The abnormal phenomenon may ascribe to the 2-D iodoplumbate anionic layer in **4** with dimensionality higher than the anionic chains in **5** and **6**, which obeys the rule that the band gap decreases as the dimensionality increases.[32] In addition, the band gaps of **1**–**6** are all consistent with their colors of the crystals, respectively.

<Please insert Fig. 7 here>

Fig. 7 Optical diffuse reflectance spectra for **1**–**6**, and bulk PbI_2.

3.4 Electronic structures calculations

To gain further insight of the optical properties of **2**–**6**, theoretical studies including band structure along with high symmetry points of the first Brillouin zone, and density of states (DOS) were performed using the CASTEP code.[33] The calculated band structures as well as DOS of **2**–**6** along certain symmetry directions are given in Fig. S11 and Fig. 8, respectively. The calculated band gaps of **2**–**6** using the local density approximation (LDA) are 2.71, 2.74, 1.78, 1.35 and 1.15 eV, which are smaller than their corresponding experimental values of 3.05, 2.85, 2.20, 2.64 and 2.16 eV, respectively. The discrepancy is due to the limitation of the DFT method that sometimes underestimates the band gap in semiconductors and insulators.[34] It can be seen from the band structure plots that compounds **2**, **4** and **6** are direct band gap materials, while compounds **3** and **5** are indirect band gap materials.

The aliphatic amines in **2**–**4**, and the aromatic pyridine-based SDAs in **5**–**6** have different contributions to the electronic structures of their corresponding hybrids. For aliphatic amines in **2**–**4**, they make nearly no or very small contributions to the frontier orbits of the hybrids, which

suggests that they influence the band gaps in an indirect way via modulating the anionic structures of the hybrids. The bands can be assigned according to total and partial densities of states (PDOS, Fig. 8). From the total and partial DOS (PDOS) diagrams (Fig. 8a), we can see that the Cs^+ ion and the en molecule in **2** make nearly no contribution to the top of the valence bands (VBs) and the bottom of the conduction bands (CBs). That is to say, the Cs^+ ions and en molecules do not involving the charge transition in **2**. The band just below the Fermi level between –3 and 0 eV is predominately derived from the contribution of the 5p state of I, mixing with a small amount of 6s and 6p states of Pb. The bottom of the conduction bands is mainly contributed by the 6p state of Pb, mixing with 5s state of I. Therefore, the optical absorptions are mainly ascribed to the charge transitions from 5p state of I to the 6p state of Pb, namely, the charge transitions mainly occur within the inorganic iodoplumbate anions.

Compounds **3** and **4** have similar electronic structures. The top of the VBs are mainly derived from the 5p state of I, mixing with small contribution of 6p state of Pb and p orbits of the SDAs (Figs. 8b and 8c). The bottom of the CBs is mostly formed by the 6p state of Pb and a small amount of 5s and 5p states of I. Accordingly, the intrinsic absorption of **3** and **4** can be mainly ascribed to the charge transitions from 5p state of I to the 6p state of Pb mixing with little charge transition between the p orbits of the SDAs and the 6p state of Pb, namely, the charge transitions mainly occur within the inorganic iodoplumbate anions accompanying with little charge transitions from aliphatic SDAs to iodoplumbate anions.

However, the aromatic organic cations in **5**–**6** influence the band gaps of the hybrid iodoplumbates in a direct way that significantly different from the aliphatic amines in **2**–**4**. As shown in Figs. 8d and 8e, compounds **5** and **6** have similar electronic structures. The VBs between –3 and 0 eV are all mainly from the contribution of 5p state of I without the contribution of the SDAs, which is similar to that in **2** and is different from those in **3** and **4**. Notably, the CBs between 0 and 3 eV are nearly entire from the contribution of the p-π* antibonding orbital of the aromatic organic dications, which is quite distinct from those in **2**–**4**, where the bottom of the CBs is constructed from the contributions of Pb and I atoms. Correspondingly, the optical absorption of **5** and **6** is mainly ascribed to the charge transitions from 5p state of I to the p-π* orbital of aromatic SDAs $(Et_2$2,2'-bipy$)^{2+}$ or $(Et_2$dpe$)^{2+}$, namely, the charge transitions mainly from the inorganic iodoplumbate polyanions to the aromatic SDAs, which is also different from that in **2**–**4**. In brief, different from aliphatic amines, the aromatic organic cations $(Et_2$2,2'-bipy$)^{2+}$ and $(Et_2$dpe$)^{2+}$ can make great contribution to the bottom of the conduction band, and modulate the band gap significantly and directly. The different contributions of aliphatic amines and aromatic organic cations to electronic structures observed here is consistent with our observations in iodoargentate hybrids.[8]

<Please insert Fig. 8a here>

(a)

<Please insert Fig. 8b here>

(b)

<Please insert Fig. 8c here>

(c)

<Please insert Fig. 8d here>

(d)

<Please insert Fig. 8e here>

(e)

Fig. 8 Total and partial density of states of **2** (a), **3** (b), **4** (c), **5** (d), and **6** (e).

3.5 Water induced structure conversions

Besides the different contributions to crystal and electronic structures, the introduction of aliphatic amines and aromatic species into iodoplumbate hybrids can also induce different stabilities in water. Compounds **1**–**4** with aliphatic amines are unstable in water and undergo structure conversions accompanying color and morphology changes (Figs. 9b and 9c). Unlike the single-crystal-to-single-crystal (SCSC) structure transformations reported in literatures, after soaked in water for 3 days the single crystallinities of as-synthesized crystals **1**–**4** are destroyed, and hence are unsuitable for single crystal X-ray diffraction studies (SXRD, Fig. 9b). In contrast, the crystals of **5** and **6** remain unchanged in water after 3 days, which suggests both compounds are stable in water (Fig. 9b).

<Please insert Fig. 9 here>

Fig. 9 The photographs of the as-synthesized single crystals of **1–6** (a), the crystals after soaked in water for 3 days (b, the samples are denoted as **1b–6b**, respectively), and the ultrasound treated samples after soaked in water for another 3 days (c, the samples are denoted as **1c–6c**, respectively).

To ensure the changes of **1**–**4** in water were thoroughly carried out, and meanwhile clarify whether any changes occurred for **5**–**6**, ultrasound treatments were performed to get fine powders of **1b**–**6b**, which were soaked in water for another 3 days to get **1c**–**6c** (Fig. 9c). Then, PXRD measurements were performed for **1c**–**6c**. The PXRD patterns of **1c** and **2c** match well with the standard pattern of the inorganic structure of PbI(OH) (Orthorhombic phase, space group *Pnma*, with lattice constants a = 7.803 Å, b = 4.204 Å, c = 10.452 Å, JCPDS No. 75-1177, Figs. 10a and 10b). For **3c**, a structure conversion can be verified by the PXRD result (Fig. S1a), however its phase confirmation is unsuccessful, and the attempt to get single crystals of **3c** suitable for SXRD study is in progress. The

PXRD pattern of **4c** matches well with the standard pattern of the inorganic structure of PbI_2 (Hexagonal phase, space group *P–3m*1, with lattice constants $a = b = 4.557$ Å, $c = 6.979$ Å, JCPDS No. 79-0803, Fig. 10c). For **5c** and **6c**, the PXRD patterns are identical with those of their corresponding as-synthesized samples, which further confirm their stabilities in water. The sharp diffraction peaks of **1c–6c** indicate good crystallinities of the samples and no other peaks related to any impurity (for **1c–2c** and **4c–6c**) were observed. Further, the structure conversions cannot be performed by soaking **1–4** in other common solvents such as ethanol, acetone, acetonitrile, ether, and chloroform. All these results suggest that water induced structure conversions from hybrid iodoplumbates to inorganic PbI(OH) or PbI_2 occurred for **1–4**. The different stabilities of compounds **1–4** from **5–6** in water are mainly ascribed to their containing aliphatic or aromatic organic species which have different hydrophilic behaviors (the NH and NH_3 groups on aliphatic amine cations of **1–4** are hydrophilic).

<Please insert Fig. 10 here>

Fig. 10 The PXRD patterns of 1 (a), 2 (b), and 4 (c) under different conditions.

A dissolution and recrystallization mechanism was proposed to explain the structure conversions of **1–4**. Generally, the dissolution and recrystallization process would result in new crystal grafts on the original crystal due to easier nucleation on the defect of the original crystal,[27d] which are in accord with the phenomenon observed for **1b–4b** (Fig. 9b). After dissolved in water, the organic species retained in water, while the inorganic species crystallized as PbI(OH) phase for **1c–2c**, and as PbI_2 phase for **4c**. Considering the existence of hydroxyls in PbI(OH) phase, a hydrolysis reaction may conducted during the crystallization of **1c** and **2c**. In order to further confirm the proposed dissolution and recrystallization mechanism, 6 mg samples of **1–4** were soaked in 20 mL H_2O respectively to verify their solubilities in water. As shown in Fig. S12, after ultrasound treatment the solvents of **1** and **2** are turbid with white precipitate of PbI(OH), which implies that the hydrolysis and crystallization are quick in solvents of **1** and **2**. While, the solvents of **3** and **4** are colorless, which suggests that both samples are completely dissolved in water and the crystallization process is slow. Then, the different behaviors of **1–4** from **5–6** in water can be disclosed in the view point of metathetical reaction equilibrium: the hydrophilia of NH and NH_3 groups on the aliphatic cations promotes the metathetical reactions that generate the dissolution of the organic aliphatic cations and the crystallization of inorganic plumbum iodides.

To our knowledge, the water induced structure conversions of metal halide hybrids from hybrid iodoplumbates to inorganic plumbum iodides have never been demonstrated in detail up to now. It is anticipated that more interesting structure conversion behaviors can be observed in the continuous study of metal halide hybrids employing aliphatic amines as SDAs.

3.6 Visible light photocatalytic degradation of organic dye

As is well-known that environmental pollution is one of the major problems threaten the existence of terrestrial lives,[35] and the sunlight provides the most abundant renewable energy source to meet mankind's future energy needs.[36] In recent years, the utilization of inorganic semiconductors as photocatalysts has received much attention due to their application in solar energy conversion and environmental purification. However, this type inorganic semiconductor-based photocatalysts also show some disadvantageous issues. For wide-band gap semiconductors e.g., TiO_2, ZnO, and SnO_2, they are only able to absorb the UV irradiation that takes up less than 5% of the solar energy, whereas narrow-band gap semiconductors e,g., Fe_2O_3, CuO, and CdS have poor photocatalytic efficiency due to their high carrier recombination rate, low oxidation, or poor photo-stability, etc.[37] Thus, the preparation of new semiconductor-based photocatalysts with improved performances is more desirable. Metal halide based hybrid is an important semiconductor material, who exhibits easily tunable band gap corresponding to absorption of visible light. They can serve as potential effective photocatalysts for dye degradation, but are less explored.

<Please insert Fig. 11 here>

Fig. 11 Photodecomposition of MO dye in solution over **5** and **6**. Left: color change photograph image of dye solutions. Right: time-dependent UV/vis spectra of MO with or without two photocatalysts.

Considering that compounds **5** and **6** are stable in water and have significant absorption in the visible light region (Fig. S13), they may use as heterogeneous photocatalysts for dye wastewater treatment under visible irradiation. Methyl orange (MO) was selected as a model dye contaminant to evaluate their photocatalytic effectiveness in the degradation of waste water. The characteristic absorption of MO at 462 nm was selected to monitor the adsorption and photocatalytic degradation process. A comparison of the photocatalytic activities of as-synthesized **5** and **6** was presented in Fig. 11. The change in the concentration of MO solution is obvious with the use of **5** and **6** as photocatalyst (Fig. S14). It is obvious that compound **5** exhibits much higher activity than **6**. When the light application time increases to 30 min, the degradation ratio of MO has already reaches 88% for **5**. The superiority of **5** in the photodegradation of MO sustained before the light application time increases to 50 min. The degradation of MO in water was finished (with a degradation ratio of 92%) only after 40 min for **5** (Fig. 11). In contrast, photocatalyst **6** has to take a little longer time for degradation of MO. The nearly full degradation time for MO in the presence of **6** is 60 min. For comparison, the photodegradation process of MO without any photocatalyst has also been studied under the same condition. From Fig. 11, it can be seen that when no catalyst was added to the system, the degradation of MO was negligible. These results clearly indicate that compounds **5** and **6** exhibit high photocatalytic efficiency for the degradation of MO dye in the presence of

H_2O_2 under visible irradiation. Photocatalyst **5** possesses higher photocatalytic activity than **6**, and the reason is probably due to their discrepancy in the band gap sizes. Photocatalyst **5** has a broader band gap than **6**, which engenders it has a more effective absorption of the visible light (Fig. S13).

In order to investigate the stability of **5** and **6** as visible light photocatalysts, the PXRD patterns of both samples after the photocatalytic degradation have been also measured. The results show that the PXRD patterns of two compounds after MO photodegradation are almost identical with those of the as-synthesized samples (Fig. S15). The photocatalytic mechanism of **5** and **6** can be explained as follows.[38] The photocatalytic properties of **5** and **6** are closely related to the production of hydroxyl radicals. Although one drop H_2O_2 was added in the dye solution, it alone was not capable of degrading dye solutions without the semiconductor photocatalysts. Under visible light irradiation, valence band of semiconductor photocatalyst, **5** or **6**, generates holes (h^+) and conduction band generates the same amount of electrons (e^-). Both electron and holes can produce hydroxyl radical that is known to have high activity to degrade dye molecules.

3.6 TGA for 1–6

The thermal stabilities of **1**–**6** were examined by TGA in a N_2 atmosphere from 30 to 1000 °C (Fig. S16). The decomposition temperatures of **1**–**6** are estimated as 138 °C, 195 °C, 327 °C, 315 °C, 246 °C, and 333 °C, respectively. Because the organic cations in **1** and **3**–**6** all act as countercations in their corresponding structures, the iodoplumbate anionic framework collapses while the removal of the organic cations.[39] For **1**, a total weight loss of about 63.2% before 506 °C maybe corresponding to the removal of one $[(Hen)_4(H_{2.5}O)_2I]I_4$ per formula (theoretical value of 66.52%). From the TGA curve of **2**, it can be seen that the neutral en ligands are lost in one main step, and the observed weight loss of 6.4% in the temperature range of 195–292 °C agrees well with the calculated value of 5.94%, and the framework start to collapse when the temperature higher than 292 °C. Between the temperature range of 327–512 °C, compound **3** shows a weight loss of 53.0%, which may be due to the decomposition of one $(H_3tepa)I_3$ per formula (theoretical value of 55.42%). TGA for **4** revealed a weight loss of 47.5% before 431 °C, which corresponds to the removal of one $(H_2aep)I_2$ per formula (calcd: 45.51%). The observed total weight loss of 34.4% for **5** between 246 and 371 °C corresponds to the removal of one $(Et_2$2,2'-bipy$)I_2$ per formula (theoretical value of 33.68%). For compound **6**, a weight loss of about 35.4 % occurs between 333 to 570 °C is ascribed to the removal of one $(Et_2dpe)I_2$ per formula (calcd: 34.90%).

4. Conclusion

In summary, by introducing two types of SDAs, aliphatic amines and aromatic organic species with different structural and physical features, into inorganic iodoplumbates, we obtained six iodoplumbate hybrids which show 0–2D structures with great structural diversity. The comparative study discloses the different contributions of aliphatic amines and aromatic organic species to the crystal and electronic structures as well as properties of iodoplumbate hybrids. Of particular interest, compounds **1**–**4** exhibit interesting water induced structure conversions, while **5** and **6** are stable in water and can be used as heterogeneous photocatalysts for dye wastewater treatment under visible irradiation. All the results of the comparative study help a lot in the controllable synthesis of metal halide hybrids with different structures and functions.

Acknowledgements

We gratefully acknowledge the financial support by the NSF of China (21201080), the NSF of Shandong Province (ZR2012BQ011). We are grateful to Prof. Dr. G.-C. Guo and Dr. G.-E. Wang at FJIRSM (Fujian Institute of Research on the Structure of Matter, Chinese Academy of Sciences) for their help in theoretical calculations and helpful discussions. We also thank Prof. Dr. X.-Y. Huang at FJIRSM for help with refining the crystal structure of **1**.

Notes and references

Key Laboratory of Chemical Sensing & Analysis in Universities of Shandong, School of Chemistry and Chemical Engineering, University of Jinan, Jinan, Shandong 250022, P. R. China

E-mail: chm_liugn@ujn.edu.cn *(G.-N. Liu),* chm_licc@ujn.edu.cn *(C. Li).*

† Electronic Supplementary Information (ESI) available: Crystallographic data, additional structural Figures, TGA curves, IR spectra, and PXRD patterns. CCDC reference number 1048272-1048277 for **1**–**6**. See DOI: 10.1039/b000000x/

1. (a) L. M. Wu, X. T. Wu and L. Chen, Coord. Chem. Rev., 2009, 253, 2787; (b) N. Mercier, N. Louvain and W. H. Bi, CrystEngComm, 2009, 11, 720; (c) M.-S. Wang, G. Xu, Z.-J. Zhang and G.-C. Guo, Chem. Commun., 2010, 46, 361.
2. P. Y. Feng, X. H. Bu and N. F. Zheng, Acc. Chem. Res., 2005, 38, 293.
3. M. Mirzaei, H. Eshtiagh-Hosseini, M. Alipour and A. Frontera, Coord. Chem. Rev., 2014, 275, 1.
4. (a) D. B. Mitzi, C. A. Feild, W. T. A. Harrison and A. M. Guloy, Nature, 1994, 369, 467; (b) P. Gao, M. Gratzel and M. K. Nazeeruddin, Energy Environ. Sci., 2014, 7, 2448.
5. (a) N. Mercier, A. L. Barres, M. Giffard, I. Rau, F. Kajzar and B. Sahraoui, Angew. Chem., Int. Ed., 2006, 45, 2100; (b) W. Q. Liao, H. Y. Ye, D. W. Fu, P. F. Li, L. Z. Chen and Y. Zhang, Inorg. Chem., 2014, 53, 11146; (c) A. Lemmerer and D. G. Billing, Dalton Trans., 2012, 41, 1146.
6. (a) G. Xu, G.-C. Guo, M.-S. Wang, Z.-J. Zhang, W.-T. Chen and J.-S. Huang, Angew. Chem., Int. Ed., 2007, 46, 3249; (b) Z.-J. Zhang, S.-C. Xiang, G.-C. Guo, G. Xu, M.-S. Wang, J.-P. Zou, S.-P. Guo and J.-S. Huang, Angew. Chem., Int. Ed., 2008, 47, 4149; (c) A. M. Goforth, M. A. Tershansy, M. D. Smith, L. Peterson, J. G. Kelley, W. J. I. DeBenedetti and H. C. zur Loye, J. Am. Chem. Soc., 2011, 133, 603; (d) T. L. Yu, L. An, L. Zhang, J. J. Shen, Y. B. Fu and Y. L. Fu, Cryst. Growth Des., 2014, 14, 3875.

7. For example see: (a) D. G. Billing and A. Lemmerer, CrystEngComm, 2007, 9, 236; (b) D. G. Billing and A. Lemmerer, New J. Chem., 2008, 32, 1736; (c) D. G. Billing and A. Lemmerer, CrystEngComm, 2009, 11, 1549; (d) A. Lemmerer and D. G. Billing, CrystEngComm, 2010, 12, 1290; (e) N. Louvain, W. H. Bi, N. Mercier, J. Y. Buzare, C. Legein and G. Corbel, Dalton Trans., 2007, 965; (f) N. Leblanc, M. Allain, N. Mercier and L. Sanguinet, Cryst. Growth Des., 2011, 11, 2064; (g) H.-H. Li, Z.-R. Chen, L.-C. Cheng, M. Feng, H.-D. Zheng and J.-Q. Li, Dalton Trans., 2009, 4888; (h) H. H. Li, Y. Y. Xing, Z. X. Lian, A. W. Gong, H. Y. Wu, Y. Li and Z. R. Chen, CrystEngComm, 2013, 15, 1721; (i) T. L. Yu, L. Zhang, J. J. Shen, Y. B. Fu and Y. L. Fu, Dalton Trans., 2014, 43, 13115; (j) L. Li, H. Chen, Y. Z. Qiao and Y. Y. Niu, Inorg. Chim. Acta, 2014, 409, 227.
8. G.-N. Liu, L.-L. Liu, Y.-N. Chu, Y.-Q. Sun, Z.-W. Zhang and C. Li, Eur. J. Inorg. Chem., 2015, 2015, 478.
9. (a) J. Li, Z. Chen, R. J. Wang and D. M. Proserpio, Coord. Chem. Rev., 1999, 190-192, 707; (b) J. Zhou, J. Dai, G. Q. Bian and C. Y. Li, Coord. Chem. Rev., 2009, 253, 1221; (c) S.-T. Zheng and G.-Y. Yang, Chem. Soc. Rev., 2012, 41, 7623.
10. (a) Z.-J. Zhang, S.-C. Xiang, Y.-F. Zhang, A.-Q. Wu, L.-Z. Cai, G.-C. Guo and J.-S. Huang, Inorg. Chem., 2006, 45, 1972; (b) A. Aquilino, M. Cannas, A. Christini and G. Marongiu, Chem. Comm., 1978, 347; (c) H. J. Haupt and F. Huber, Z. Anorg. Allg. Chem., 1978, 442, 31; (d) J. W. Cai, J. Myrczek and I. Bernal, Chem. Comm., 1992, 1147; (e) J. W. Cai, J. Myrczek and I. Bernal, J. Chem. Soc., Dalton Trans., 1995, 611; (f) J. M. Harrowfield, H. Miyamae, T. M. Shand, B. W. Skelton, A. A. Soudi and A. H. White, Aust. J. Chem., 1996, 49, 1043; (g) H.-H. Li, L.-G. Sun, Z.-R. Chen, Y.-J. Wang and J.-Q. Li, Aust. J. Chem., 2008, 61, 391; (h) Y. Cho, S. Kim, S. Pyo, Y. S. Park, S. J. Kim, H. Yun and J. Do, Polyhedron, 2010, 29, 2105.
11. Although we have tried our best to vary the reaction conditions, as depicted in scheme 1 in the synthetic considerations section, not all the aliphatic chelating polyamine cations were successfully incorporated into iodoplumbate systems.
12. (a) M. D. Segall, P. J. D. Lindan, M. J. Probert, C. J. Pickard, P. J. Hasnip, S. J. Clark and M. C. Payne, J. Phys.: Condens. Matter, 2002, 14, 2717; (b) V. Milman, B. Winkler, J. A. White, C. J. Pickard, M. C. Payne, E. V. Akhmatskaya and R. H. Nobes, Int. J. Quantum Chem., 2000, 77, 895.
13. D. R. Hamann, M. Schluter and C. Chiang, Phys. Rev. Lett., 1979, 43, 1494.
14. Agilent, CrysAlisPro. Version 1.171.35.21 ed.; Agilent Technologies Corp.: California, America.
15. Siemens, SHELXTL Version 5 Reference manual. Siemens Energy & Automaion Inc.: Madision,WI, 1994.
16. X.-M. Zhang, Coord. Chem. Rev., 2005, 249, 1201.
17. (a) J. B. Parise and Y. H. Ko, Chem. Mater., 1992, 4, 46; (b) A. V. Powell, R. Paniagua, P. Vaqueiro and A. M. Chippindale, Chem. Mater., 2002, 14, 1220; (c) G.-M. Wang, Y.-Q. Sun and G.-Y. Yang, J. Solid State Chem., 2005, 178, 729; (d) Y.-J. Zhong, Y.-M. Chen, Y.-Q. Sun and G.-Y. Yang, Z. Anorg. Allg. Chem., 2005, 631, 1957; (e) S.-T. Zheng, M.-H. Wang and G.-Y. Yang, Inorg. Chem., 2007, 46, 9503; (f) J. Zhou, Y. Zhang, G. Q. Bian, C. Y. Li, X. X. Chen and J. Dai, Cryst. Growth Des., 2008, 8, 2235; (g) G.-N. Liu, G.-C. Guo, M.-S. Wang, L.-Z. Cai and J.-S. Huang, J. Mol. Struct., 2010, 983, 104; (h) S. Satapathi, S. Choubey, K. Bhar, S. Chattopadhyay, P. Mitra, A. M. Z. Slawin and B. K. Ghosh, Inorg. Chim. Acta, 2012, 384, 37.
18. G. A. Mousdis, V. Gionis, G. C. Papavassiliou, C. P. Raptopoulou and A. Terzis, J. Mater. Chem., 1998, 8, 2259.
19. (a) N. Louvain, N. Mercier, J. Luc and B. Sahraoui, Eur. J. Inorg. Chem., 2008, 3592; (b) G.-E. Wang, X.-M. Jiang, M.-J. Zhang, H.-F. Chen, B.-W. Liu, M.-S. Wang and G.-C. Guo, CrystEngComm, 2013, 15, 10399; (c) A. Wakamiya, M. Endo, T. Sasamori, N. Tokitoh, Y. Ogomi, S. Hayase and Y. Murata, Chem. Lett., 2014, 43, 711.
20. (a) Z.-J. Zhang, G.-C. Guo, G. Xu, M.-L. Fu, J.-P. Zou and J.-S. Huang, Inorg. Chem., 2006, 45, 10028; (b) A. Lemmerer and D. G. Billing, CrystEngComm, 2012, 14, 1954.
21. (a) D. B. Mitzi, D. R. Medeiros and P. R. L. Malenfant, Inorg. Chem., 2002, 41, 2134; (b) T. L. Yu, J. J. Shen, Y. B. Fu and Y. L. Fu, CrystEngComm, 2014, 16, 5280.
22. H.-H. Li, Z.-R. Chen, L.-C. Cheng, J.-B. Liu, X.-B. Chen and J.-Q. Li, Cryst. Growth Des., 2008, 8, 4355.
23. (a) J. Calabrese, N. L. Jones, R. L. Harlow, N. Herron, D. L. Thorn and Y. Wang, J. Am. Chem. Soc., 1991, 113, 2328; (b) D. B. Mitzi, Chem. Mater., 1996, 8, 791; (c) X. H. Zhu, N. Mercier, A. Riou, P. Blanchard and P. Frere, Chem. Commun., 2002, 2160; (d) N. Mercier, CrystEngComm, 2005, 7, 429.
24. X. H. Zhu, N. Mercier, P. Frere, P. Blanchard, J. Roncali, M. Allain, C. Pasquier and A. Riou, Inorg. Chem., 2003, 42, 5330.
25. (a) Y. Shi, L. H. Li, Y. Z. Li, Y. Xu, X. T. Chen, Z. L. Xue and X. Z. You, Inorg. Chem. Commun., 2002, 5, 1090; (b) L. Y. Kong, Z. H. Zhang, T. A. Okamura, M. J. Fei, W. Y. Sun and N. Ueyama, Chem. Lett., 2004, 33, 1572; (c) Y.-J. Wang, H.-H. Li, Z.-R. Chen, C.-C. Huang, X.-H. Huang, M. Feng and Y. Lin, CrystEngComm, 2008, 10, 770; (d) H. X. Guo, X. Z. Li, W. Weng, Q. H. Wang, W. B. Wu, M. Liang, C. Q. Zheng and B. Lin, Chin. J. Struc. Chem., 2009, 28, 283; (e) J. Liu, H.-H. Li, Z.-R. Chen, L.-Q. Guo, C.-C. Huang and J.-Q. Li, CrystEngComm, 2009, 11, 545; (f) H.-H. Li, Z.-R. Chen, L.-C. Cheng, Y.-J. Wang, M.-A. Feng and M. Wang, Dalton Trans., 2010, 39, 11000.
26. (a) S. M. Wang, D. B. Mitzi, C. A. Feild and A. Guloy, J. Am. Chem. Soc., 1995, 117, 5297; (b) X. H. Zhu, N. Mercier, M. Allain, P. Frere, P. Blanchard, J. Roncali and A. Riou, J. Solid State Chem., 2004, 177, 1067; (c) G. C. Papavassiliou, G. A. Mousdis, C. P. Raptopoulou and A. Terzis, Z. Naturforsch. B, 1999, 54, 1405.
27. For recent publications, please see: (a) Y. Chen, Z. Yang, C. X. Guo, C. Y. Ni, H. X. Li, Z. G. Ren and J. P. Lang, CrystEngComm, 2011, 13, 243; (b) S. Mishra, E. Jeanneau, O. Iasco, G. Ledoux, D. Luneau and S. Daniele, Eur. J. Inorg. Chem., 2012, 2749; (c) G.-E. Wang, M.-S. Wang, X.-M. Jiang, Z.-F. Liu, R.-G. Lin, L.-Z. Cai, G.-C. Guo and J.-S. Huang, Inorg. Chem. Commun., 2011, 14, 1957; (d) G.-E. Wang, G. Xu, P.-X. Li, S.-H. Wang, M.-S. Wang, G.-C. Guo and J.-S. Huang, CrystEngComm, 2013, 15, 2579; (e) H. R. Zhao, D. P. Li, X. M. Ren, Y. Song and W. Q. Jin, J. Am. Chem. Soc., 2010, 132, 18; (f) J. J. Zhao, Y. N. Wang, H. L. Jia, J. H. Yu and J. Q. Xu, J. Cluster Sci., 2014, 25, 571; (g) H.-H. Li, Y.-J. Wang, Z.-X. Lian, Y.-F. Xu, M. Wang, S.-W. Huang and Z.-R. Chen, J. Mol. Struct., 2012, 1016, 118; (h) W. X. Chai, J. Lin, L. Song, L. S. Qin, H. S. Shi, J. Y. Guo and K. Y. Shu, Solid State Sci., 2012, 14, 1226.

28. (a) X. B. Chen, H. H. Li, Z. R. Chen, J. B. Liu, J. B. Li, H. J. Dong and Y. L. Wu, J. Cluster Sci., 2009, 20, 611; (b) L. Q. Fan, J. H. Wu and Y. F. Huang, J. Solid State Chem., 2007, 180, 3479; (c) L. Q. Fan, L. Chen and L. M. Wu, Acta Crystallogr., Sect. E: Struct. Rep. Online, 2006, 62, M3373.
29. (a) V. N. Kokozay and A. V. Sienkiewicz, Polyhedron, 1995, 14, 1547; (b) G. A. Bowmaker, J. M. Harrowfield, H. Miyamae, T. M. Shand, B. W. Skelton, A. A. Soudi and A. H. White, Aust. J. Chem., 1996, 49, 1089; (c) H. G. Zhu, Y. Xu, Z. Yu, Q. J. Wu, H. K. Fun and X. Z. You, Polyhedron, 1999, 18, 3491; (d) J. S. Casas, E. E. Castellano, J. Ellena, M. S. Garcia-Tasende, A. Sanchez, J. Sordo and M. J. Vidarte, Main Group Met. Chem., 2001, 24, 455.
30. Y. Y. Niu, H. W. Hou and Y. Zhu, J. Cluster Sci., 2003, 14, 483.
31. A. J. Blake, N. R. Brooks, N. R. Champness, P. A. Cooke, M. Crew, A. M. Deveson, L. R. Hanton, P. Hubberstey, D. Fenske and M. Schröder, Cryst. Eng., 1999, 2, 181.
32. G. C. Papavassiliou, Prog. Solid State Chem., 1997, 25, 125.
33. Although tried many times, the theoretical calculation on **1** was still unsuccessful.
34. (a) R. W. Godby, M. Schluter and L. J. Sham, Phys. Rev. B, 1987, 36, 6497; (b) C. M. I. Okoye, J. Phys.-Condens. Mat., 2003, 15, 5945.
35. J. G. Hou, C. Yang, Z. Wang, S. Q. Jiao and H. M. Zhu, Appl. Catal., B, 2013, 129, 333.
36. L. Hammarstrom and S. Hammes-Schiffer, Acc. Chem. Res., 2009, 42, 1859.
37. (a) D. Chatterjee and S. Dasgupta, J. Photochem. Photobiol., C, 2005, 6, 186; (b) C. C. Wang, J. R. Li, X. L. Lv, Y. Q. Zhang and G. S. Guo, Energy Environ. Sci., 2014, 7, 2831; (c) X. S. Zhai, Y. Q. Zheng, J. L. Lin and W. Xu, Inorg. Chim. Acta, 2014, 423, 1.
38. (a) Z. Li, L. W. Mi, W. H. Chen, H. W. Hou, C. T. Liu, H. L. Wang, Z. Zheng and C. Y. Shen, CrystEngComm, 2012, 14, 3965; (b) T. Wen, D. X. Zhang and J. Zhang, Inorg. Chem., 2013, 52, 12.
39. (a) H. H. Li, Z. R. Chen, J. Q. Li, C. C. Huang, Y. F. Zhang and G. X. Jia, Eur. J. Inorg. Chem., 2006, 2447; (b) Y. Z. Qiao, W. Z. Fu, J. M. Yue, X. C. Liu, Y. Y. Niu and H. W. Hou, CrystEngComm, 2012, 14, 3241.

Graphical Abstract

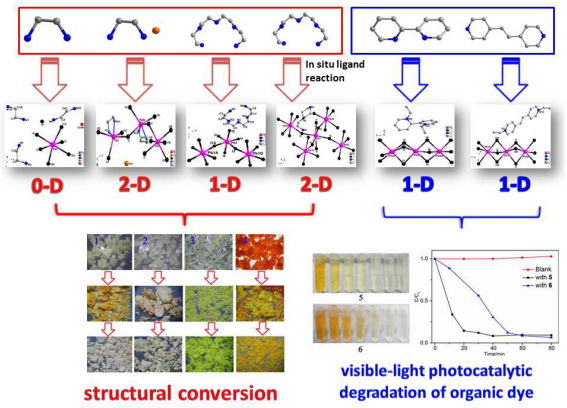

A comparative study was performed to disclose the different contributions of aliphatic and aromatic structure directing agents to the crystal and electronic structures, and property of iodoplumbate hybrids.

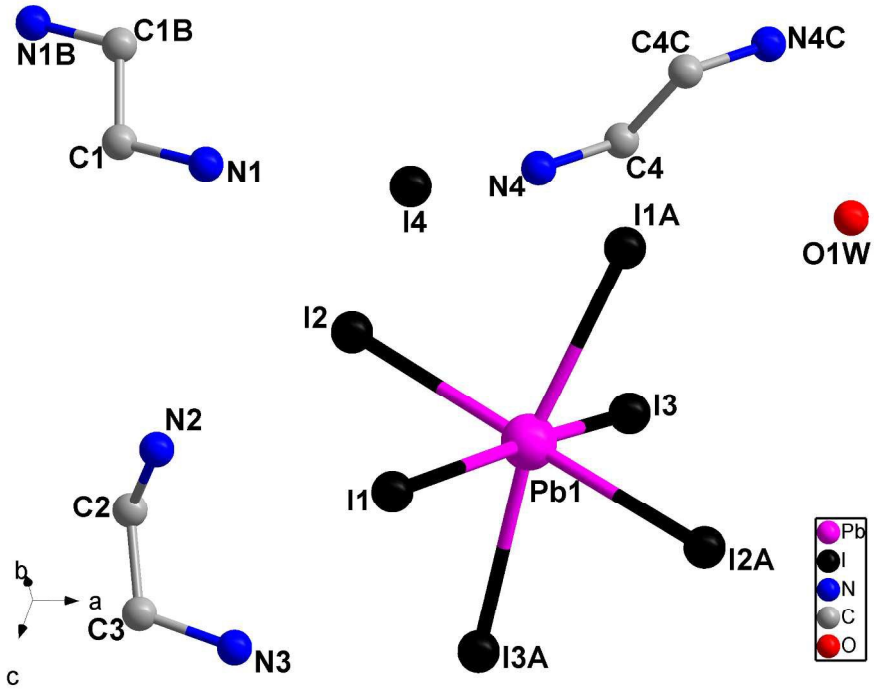

661x495mm (96 x 96 DPI)

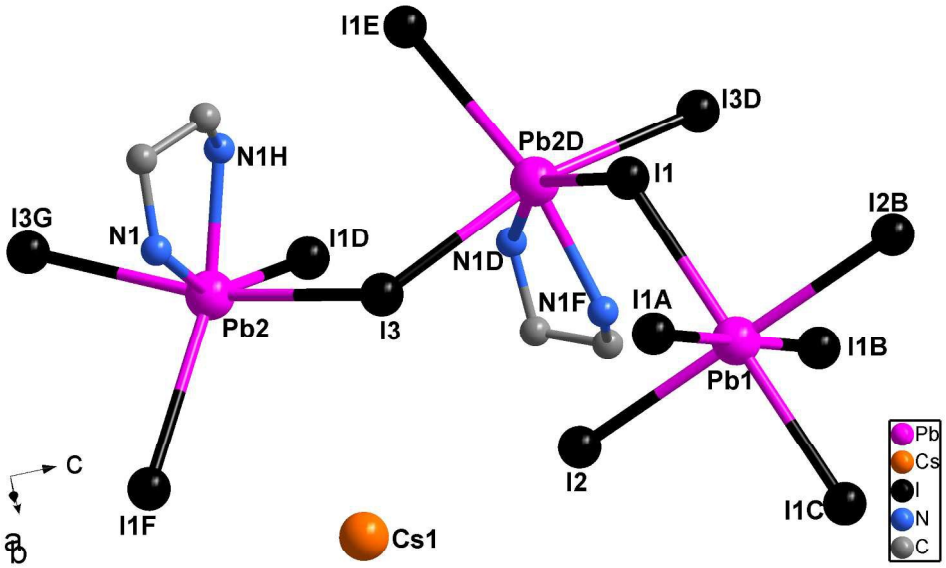

661x495mm (96 x 96 DPI)

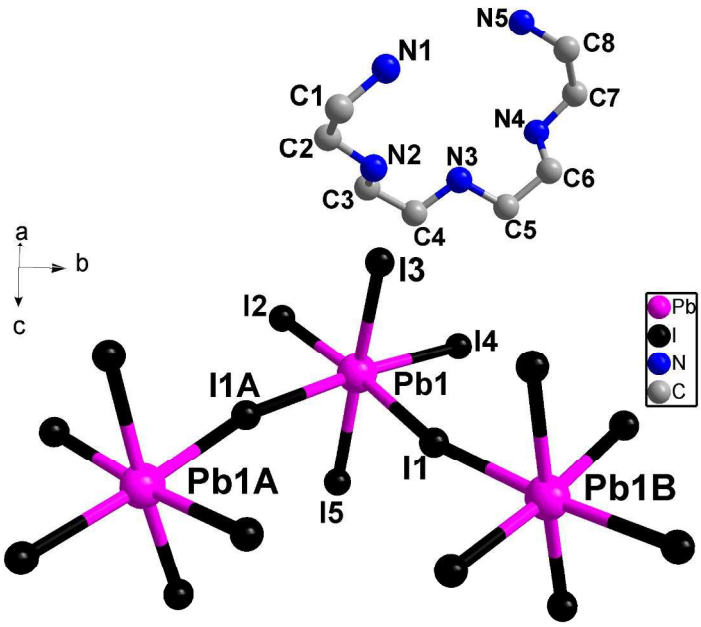

661x495mm (96 x 96 DPI)

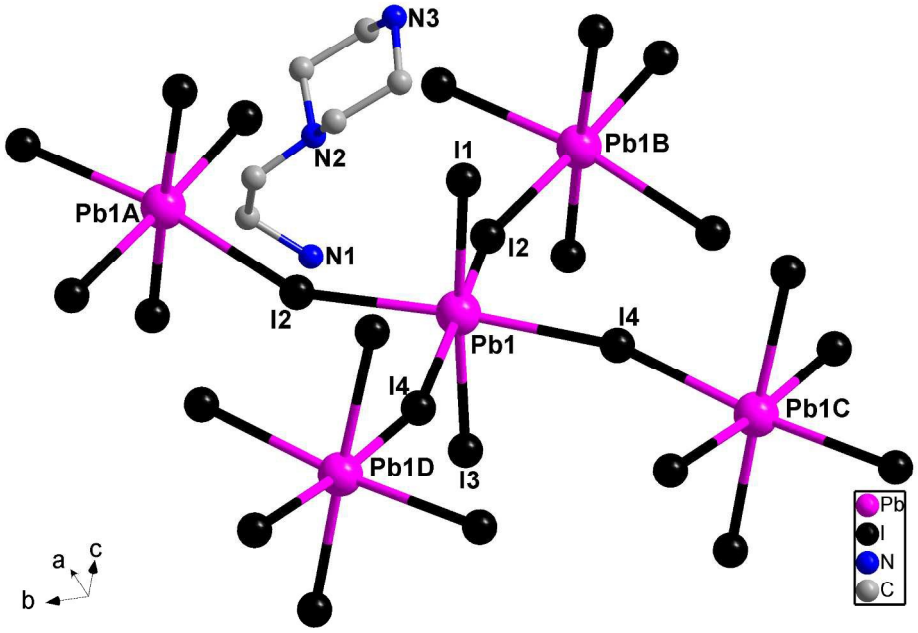

661x495mm (96 x 96 DPI)

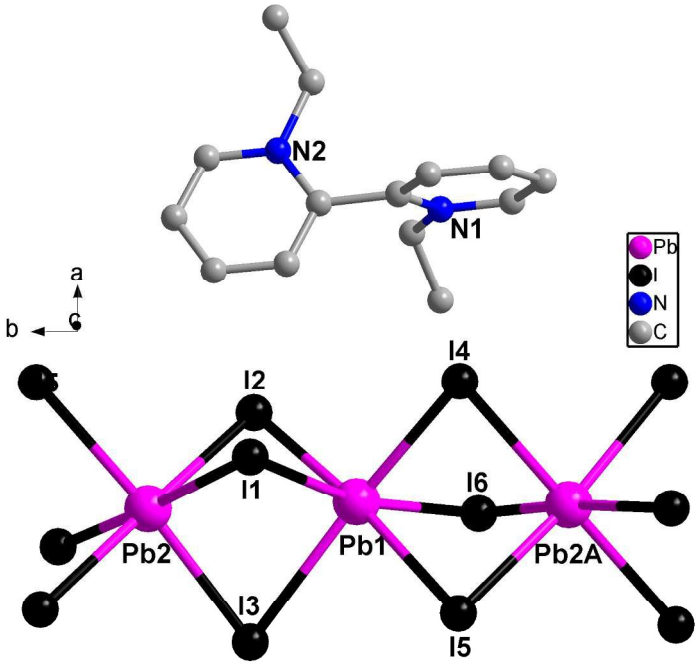

661x495mm (96 x 96 DPI)

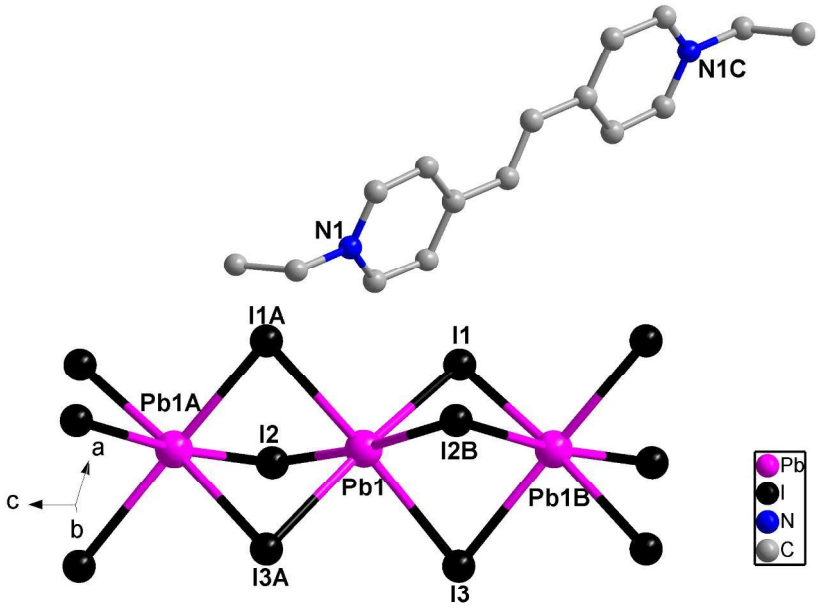

661x495mm (96 x 96 DPI)

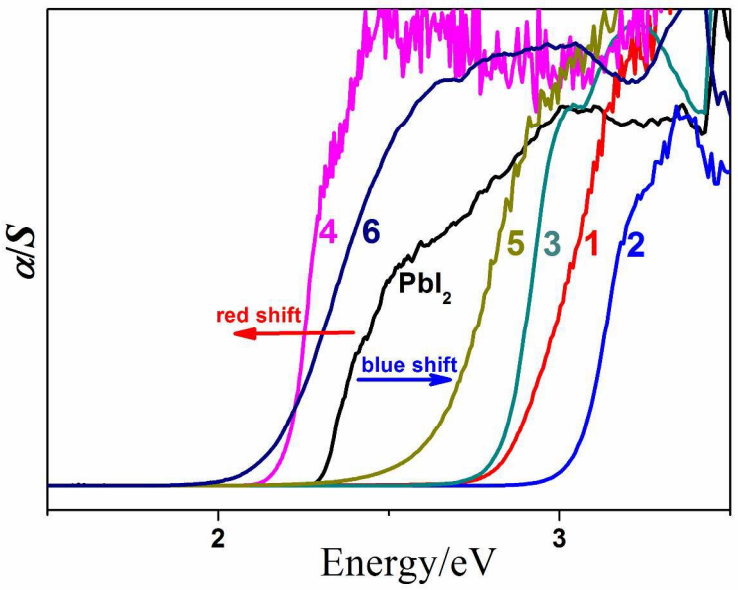

288x201mm (300 x 300 DPI)

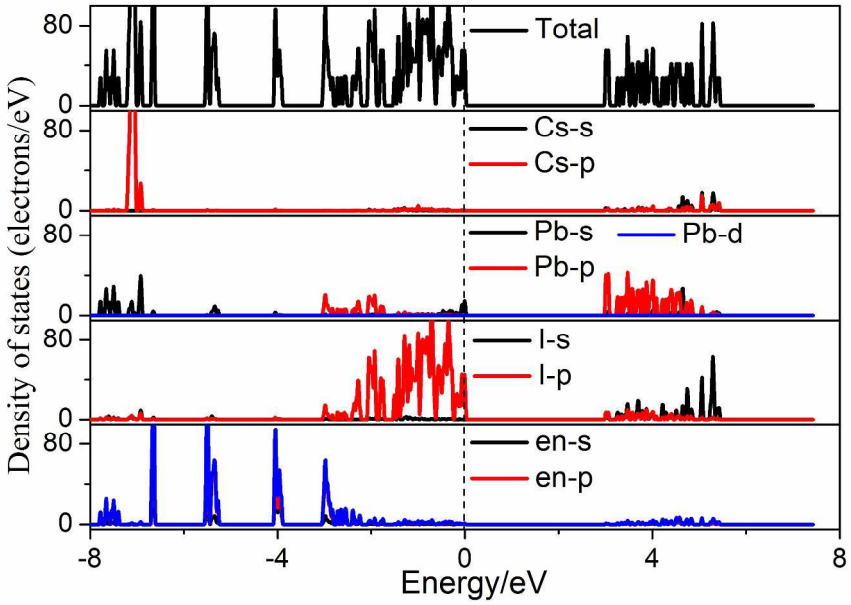

289x202mm (300 x 300 DPI)

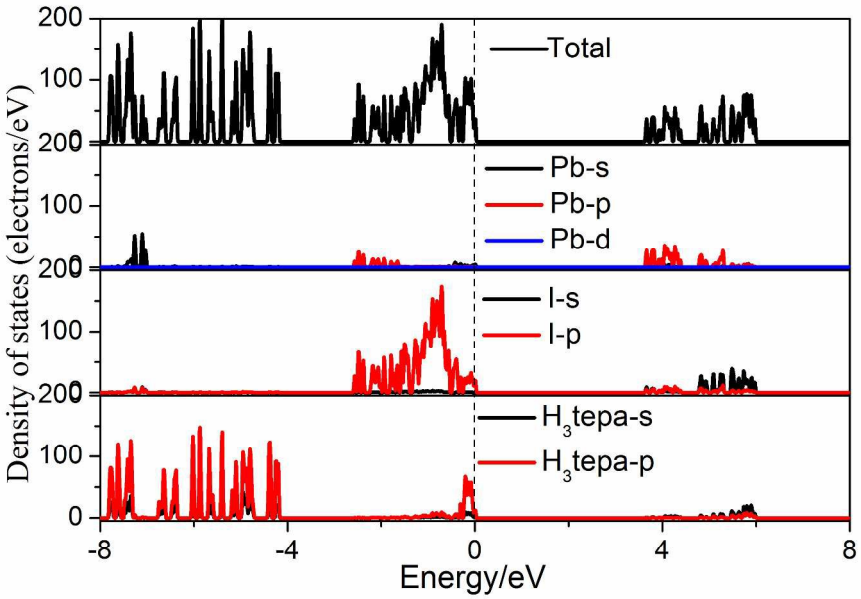

289x202mm (300 x 300 DPI)

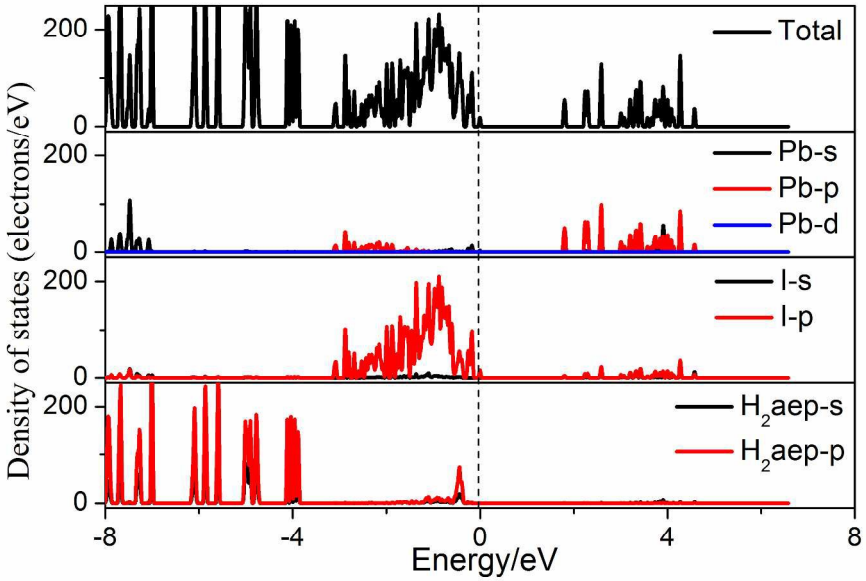

289x202mm (300 x 300 DPI)

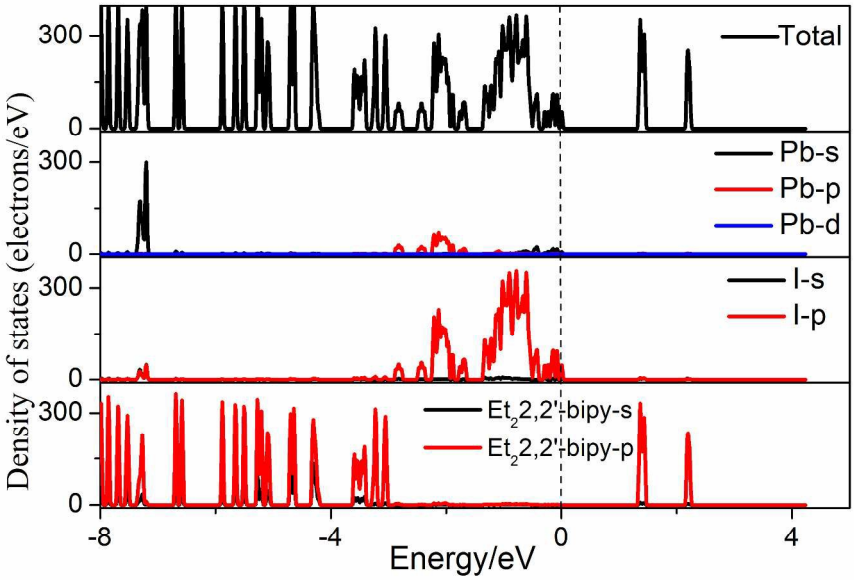

289x202mm (300 x 300 DPI)

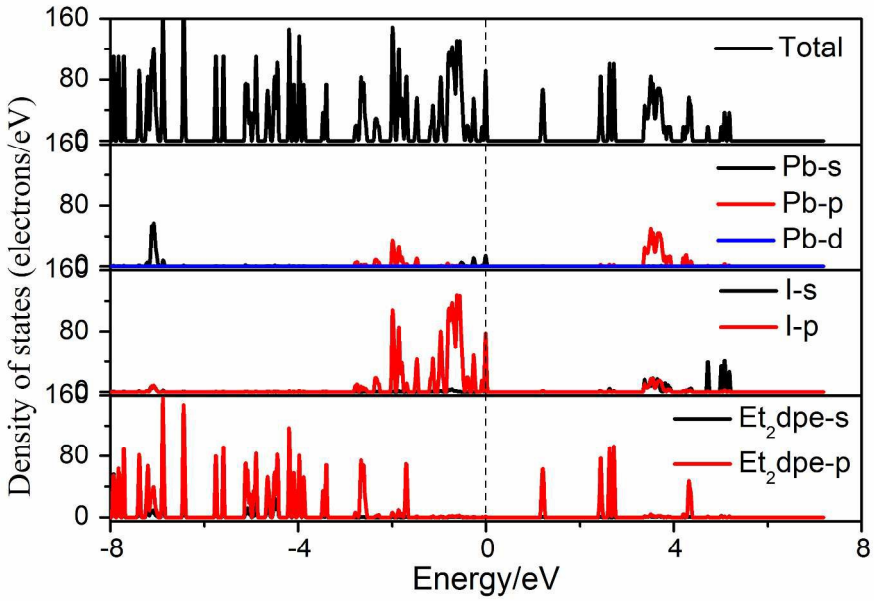

288x201mm (300 x 300 DPI)

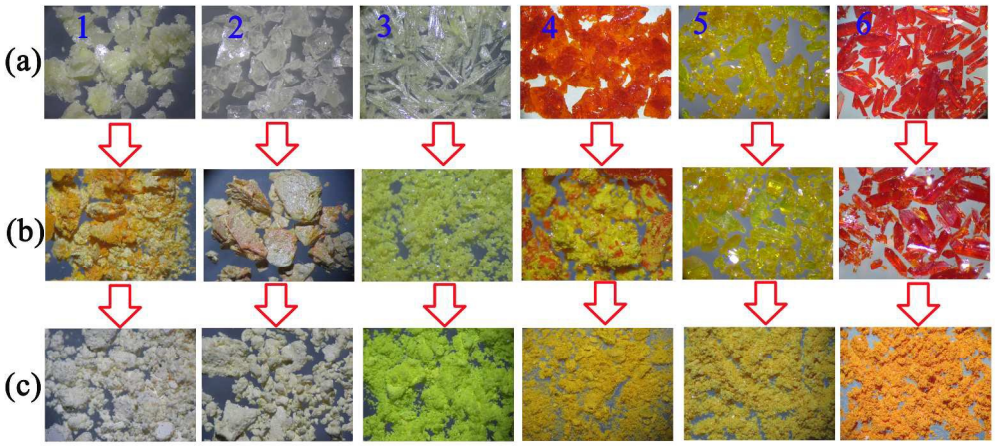

398x180mm (300 x 300 DPI)

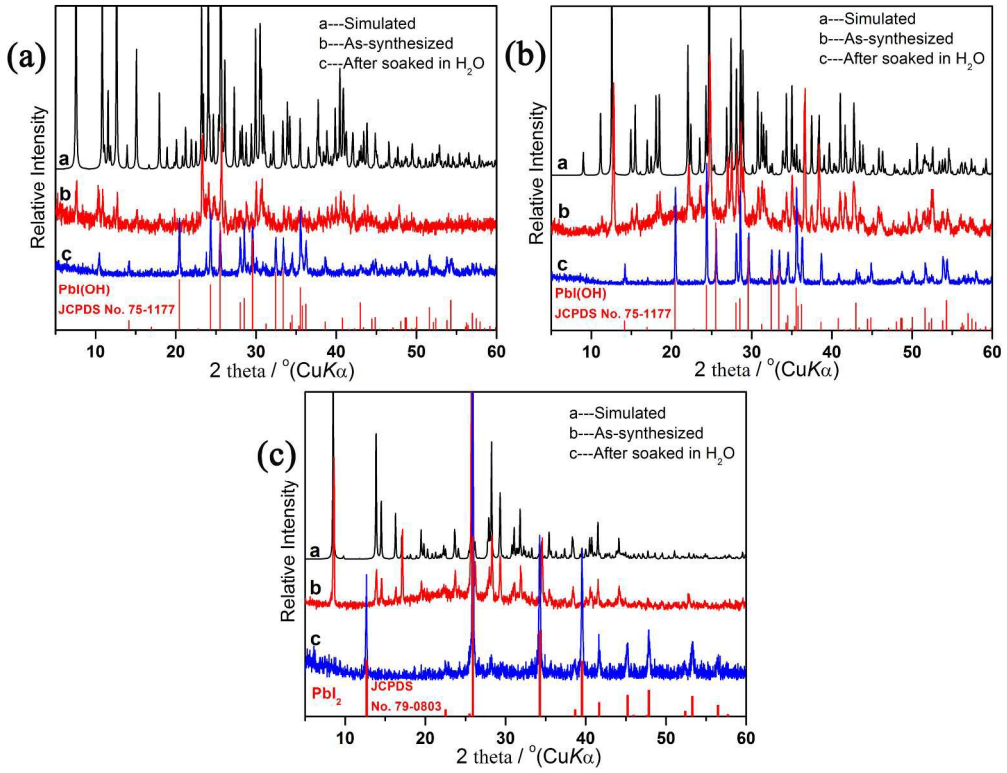

247x192mm (300 x 300 DPI)

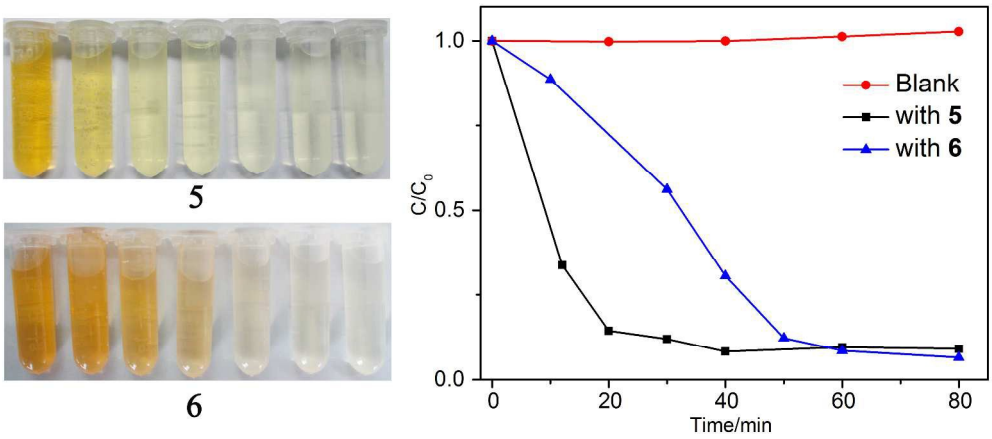

388x168mm (300 x 300 DPI)

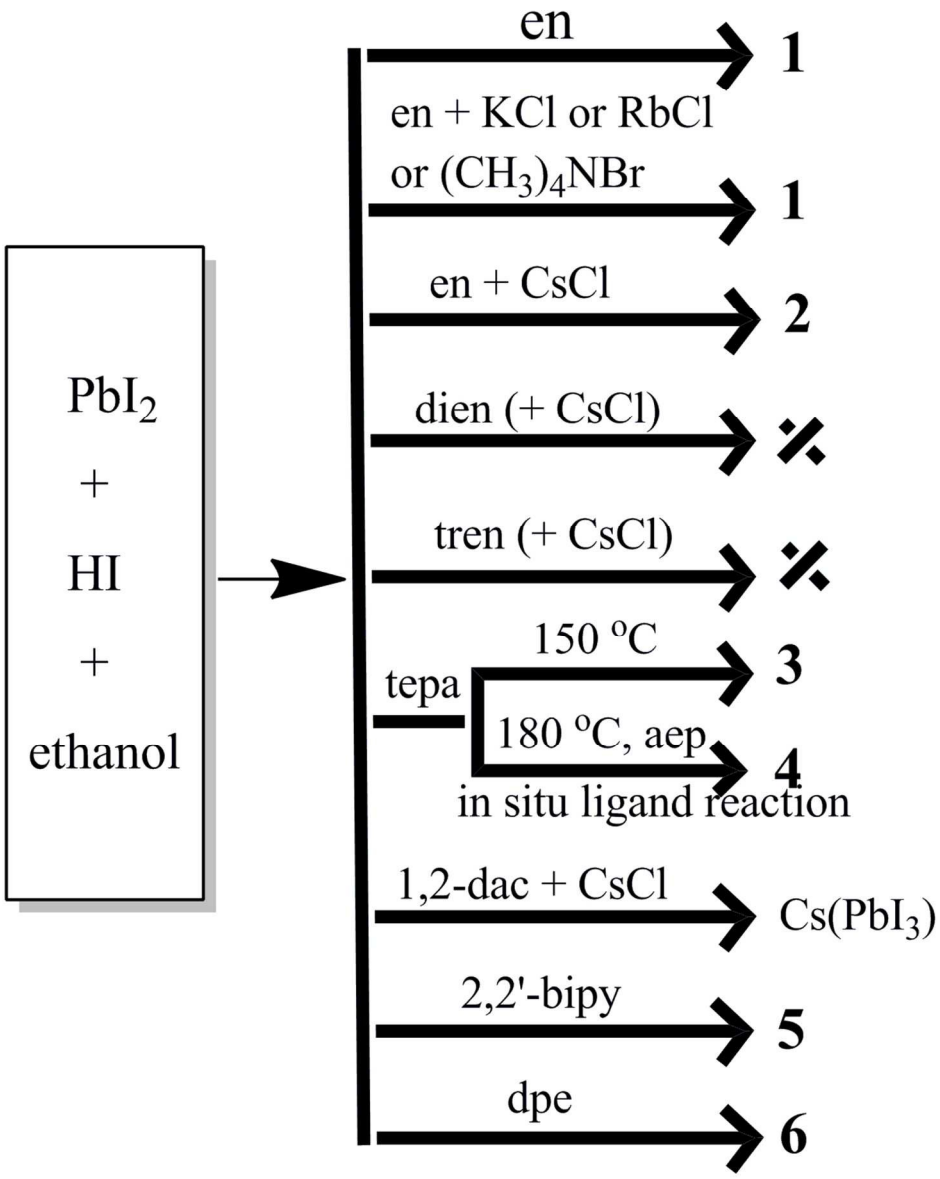

103x130mm (300 x 300 DPI)

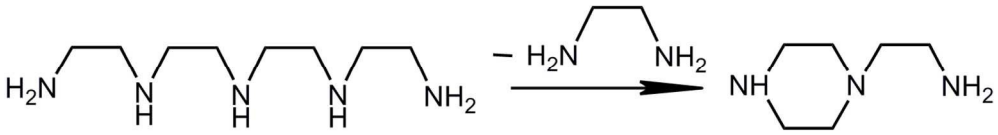

124x16mm (300 x 300 DPI)